MECHANICAL DAMAGE REVIEW

Eric Samson
Email: esamson@simcotechnologies.com
SIMCO Technologies, Inc.
Quebec City, Canada

and

Sohini Sarkar
Email: sohini.sarkara@vanderbilt.edu
David S. Kosson
Email: david.kosson@vanderbilt.edu
Vanderbilt University, School of Engineering
Consortium for Risk Evaluation with Stakeholder Participation, III
Nashville, Tennessee 37235

November 2009
CBP-TR-2009-002, Rev. 0

CONTENTS **PageNo.**

CONTENTS (contd) **Page No.**

CONTENTS (contd) **Page No.**

LIST OF FIGURES **Page No.**

LIST OF TABLES

LIST OF ABBREVIATIONS AND ACRONYMS

ACI	American Concrete Institute
ASH	Alkali-Silicate-Hydrate
ASR	Alkali Silica Reaction
CH	Calcium Hydroxide
C-S-H	Calcium Silicate Hydrate
DT	Destructive Test
HPC	High-Performance Concrete
HPFC	High-Performance steel Fiber-reinforced Concrete
IE	Impact Echo
MASW	Multiple Impact Surface Waves
MCSC	Maximum circumferential stress criterion
MD	Molecular Dynamic
MSEDC	Minimum strain energy density criterion
MSERRC	Maximum strain energy release rate criterion
NDT	Nondestructive Test
NMR	Nuclear Magnetic Resonance
OC	Ordinary Concrete
RVE	Representative Volume Element
SASW	Spectral Analysis of Surface Waves
SEM	Scanning Electron Microscopy
SIR	Slab Impulse Response
XRD	X-Ray Diffraction

LIST OF SYMBOLS

a	Ratio of damaged/total material surface
a_c	Mean half crack length
a_l	Chemical activity
A_c	Material characteristic in F/T fatigue
A / A_0	Effective/total surface
A_H	Coefficient for normalized affinity of hydration
A_ξ	Initial affinity of the hydration reaction
b	Biot coefficient
b_0	Available fraction of porosity
B_c	Material characteristic in F/T fatigue
c	Concrete cover thickness
C	Weighted average of the chemical concentration
C_d	Crack density
$c_p^{\,s} / c_p^{\,l}$	Ice/water heat capacity
C_t	Total chloride content
$\mathbf{C}_\xi^t$	Elasticity stiffness tensor of hydration
d	Damage parameter
D	Diffusion coefficient
d_0	Thickness of high porous concrete zone
d_c	Deformation induced by rust production
d_{cr}	Model parameter of damaged diffusion coefficient
$D_d / D_0 / D_{max}$	Damaged/initial undamaged/maximum value of the diffusion coefficient
D_C	Diffusion coefficient in the cracks
D_p	Conduction percolation threshold
e	Characteristic of damageable material
E	Young's modulus
E_0	Undamaged dynamic Young's modulus
E_a	Activation energy
E_{ef}	Effective Young's modulus
E_n	Damaged dynamic Young's modulus
E_r	Young's modulus of rust product

LIST OF SYMBOLS (contd)

F	Faraday's constant
F_0/F_f	Solution/Saturated material conductivity
f'_c	Ultimate compressive strength
f^d	Damage criteria
f^I	Inclusion volume density
f_t	Tensile strength of concrete
f_ξ	Source term to model the heat of hydration
g_{ct}	Constant for Young's modulus calculation during hydration
h_0^{ls}	Enthalpy of ice formation
I	Unit matrix
I_{cor}	Corrosion current density
i_{cor}	Mean annual corrosion rate
J_r	Corrosion rate
k	Reaction rate constant
K	Intrinsic permeability
k_0	Characteristic of the ASR chemical process
$K_{V(0)}/K_{V(d)}$	Initial/damaged gas permeability
K_g	ASR gel stiffness
K_I	Stress intensity factor
K_N	Coefficient of fatigue in F/T damage
K_r	Stiffness of rust product
L	Length
l_r	Thickness of adsorbed liquid layer
m	Weibull's law parameter
M	Molar concentration
m_C	Steel bar – concrete cover coefficient in corrosion model
M_{crit}	Critical corrosion mass products
m_{Fe}	Equivalent iron mole

LIST OF SYMBOLS (contd)

M_P	Corrosion mass products filling the porous ring around steel bar
m_r	Corrosion produced mass
m_{RH}	Model parameter of ASR gel pressure
M_S	Corrosion mass products introducing the crack
M_{st}	Steel bar mass consumed by corrosion
n	Model parameter of damaged diffusion coefficient
$n_0/n_1/n_2$	Material constant in the hydration model
N	Total molar concentration
n_V	Ratio of the rust volume on initial steel volume
p	Pressure
P_C	Pressure inside of concrete cover
P_g	ASR gel pressure
P_l	Pressure of liquid phase
P_{ice}	Pressure due by ice formation
P_r	Pressure induced by corrosion product
Pf^{ASR}	Cracking probability
P^n	Pressure exerted by the chemical expanding
p_v/p_{vs}	Normal / saturated vapor pressures
q	Equivalent stoichiometric coefficient
Q_ξ	Material parameter in the heat of hydration model
r_0/r_1	Characteristics of material in damage criteria
R	Gas constant
R_0	Radius of steel bar plus concrete cover
r_{a0}	Initial radius of the calcium particle
R_c	Radius of damaged zone induced by rust production
R_{eq}	Equivalent pore radius
RH	Relative humidity
R_i	Initial radius of the steel bar plus high porous concrete zone
R_s	Initial radius of the steel bar
R_r	Ohmic resistance of the cover concrete

LIST OF SYMBOLS (contd)

S	Ratio of un-cracked on cracked surface of material
S_{cr}	Critical degree of saturation
S_r	Critical degree of saturation
$S(\omega)$	Matrix of the degradation properties of material
t	Time
T	Temperature
U	Concentration
V	Volume
V_C	Volume or corrosion product
V_R	Volume of original steel
V_s	Volume of solid
w/w_h	Effective /equivalent crack width
w_c	Specific weight of concrete
W	Equivalent weight of steel
W_c	Water content of concrete
W_l	Moisture loss of concrete
W_t	Consumed water for hydration at time t
W_∞	Consumed water for fully hydration
x_{unf}	Molar fraction
z	Ionic valence of iron
α	Characteristic of damageable material
α_f	Constant for compressive calculation during hydration
α_ε	Material constant to calculate ASR part of strain
α_T	Concrete thermal coefficient of expansion.
α_T^ξ	Thermal expansion parameter associated with the heat of hydration
α_1/α_2	Corrosion mass characteristic coefficients
β	Characteristic of damageable material
β_f	Constant for compressive calculation during hydration

LIST OF SYMBOLS (contd)

δ	F/T damage
ε / ε^e/ ε^{pl} / ε^{ASR} / ε^+	Total/elastic/plastic/ASR/positive part of strain
ε^{**}	Eigenstrain
ε^{ch}	Chemical strain
ε^c	Creep strain
ε^H	Hydration strain
ε^o	Autogenous strain
ε^{sh}	Shrinkage strain
ε^T	Thermal strain
ε_v	Volumetric strain
ϕ/ϕ_0	Effective/initial porosity
γ	Characteristic of damageable material
γ_c	Rate of saturation increasing in F/T fatigue
γ_{ls}	Liquid/solid surface tension
φ	Porosity of chemical products
φ_{cap}	Capillary fraction of porosity
$\varphi(r)$	Pore size distribution
κ_1/κ_2	Experimental parameters describing effect of damage on gas perm.
κ_e/κ_p	Constants related to crack and porosity in ASR gel pressure model
κ_C	Rust production rate
λ	Coefficient of Lamé
λ_d	Damage coefficient
μ	Coefficient of Lamé
μ_ω	Exponent for a three-dimensional diffusion coefficient
ν	Poisson's ratio

LIST OF SYMBOLS (contd)

v_s/v_l	Ice formation/water specific volume of
v_r	Poisson's ratio of rust product
θ	Creep coefficient
ρ_r	Mass density of corrosion products
μ_s	Mass density original steel
$\sigma/\sigma'/\sigma_g$	Total/effective/undamaged material stress
σ_r	Residual stress
σ_t	Tangential stress
σ_u	Weibull's law parameter
τ_C	Empirical parameter which describing the cracks' roughness
ω	Damage due to sulfate attack
ξ	Degree of hydration
ξ_∞	Maximum degree of hydration
ψ_e	Function of elastic free energy

MECHANICAL DAMAGE REVIEW

Eric Samson
SIMCO Technologies, Inc.
Quebec City, Canada

Sohini Sarkar
David S. Kosson
Vanderbilt University, School of Engineering
Consortium for Risk Evaluation with Stakeholder Participation, III
Nashville, TN 37235

ABSTRACT

This report summarizes modeling approaches used to predict the formation of cracks in cementitious materials. General considerations related to cracks such as the origin, detection, and prevention are first outlined.

Following this, a section is dedicated to the general description of approaches to model the formation of cracks in materials. The first method reviewed is called damage mechanics. It is based on a damage parameter that indicates the level of damage in a continuous material. The second method is called the fracture mechanics. In this approach, the geometry and localization of cracks is predicted instead of relying on a smeared damage parameter.

The other sections are dedicated to the description of models developed for specific damage phenomena. Early age cracking caused by the heat generated during the hydration process and the drying shrinkage is first discussed. This is followed by reviews on damage models dealing with sulfate ingress in concrete, rebar corrosion, alkali-silica reaction and freezing/thawing cycles.

1.0 INTRODUCTION

Many degradation problems affecting concrete structures have their origin in ionic, energy, and moisture exchanges between the material and the surrounding environment. For example, the exchange of ions at the material/environment interface initiates chemical reactions due to the chemical imbalance between the pore solution and the hydrated cement paste, and the exchange of energy associated with temperature variations in the environment can trigger the formation of ice crystals in the pores.

Most of these internal modifications to the material are not macroscopically apparent at the time of initiation. But ultimately, the chemical and physical alterations to the microstructure translate into internal stresses and can lead to the formation of cracks. Once the material is cracked, structural elements no longer perform according to their original design. Also, the formation of cracks marks an increase in the degradation rate of the material due to the increased ionic and moisture exchange rates through these high permeability paths.

Good construction practices can help prevent many of these problems in conventional structures. For instance, designing a concrete mixture with the proper amount of air entraining agent and non reactive aggregates should protect the structure from freezing/thawing and alkali-silica reaction damages in all but the most severe environments. When the material is put in place, good curing practices will prevent drying shrinkage and surface cracking. Selecting low water-to-binder ratio and low permeability concretes in chloride- or sulfate-laden environments will slow the ingress of contaminants and ensure a long service-life.

The case of nuclear waste storage structures poses additional challenges to durability concerns, mainly because of the very long service-life (1000+ years) that is expected. With these structures, the objective of properly designing the concrete mixture is not to prevent cracking but to control it, because crack-free scenarios can hardly be expected over such long timeframes. Models that can predict the formation and propagation of cracks as a function of microstructure alteration and external conditions are thus valuable design tools for this specific application.

This report reviews mechanical damage models found in the literature that address the most common degradation problems. The first sections summarize the formation of cracks in concrete and general mechanical damage models. This is followed by a review of damage models for selected degradation phenomena: sulfate attack, rebar corrosion, alkali-silica reaction, and freezing and thawing damages.

2.0 GENERAL OVERVIEW OF DAMAGE IN CONCRETE

2.1 Causes of Damage in Concrete

This section summarizes the causes leading to cracks in concrete. Most of the text is taken from the ACI Concrete Repair Manual 224.1R-07 (2007).

2.1.1 Cracking of Plastic Concrete

Plastic concrete in this report refers to fresh concrete. (For more details, see the report chapter “Early-Age Cracking Review: Mechanisms, Material Properties, and Mitigation Strategies.”)

2.1.1.1 Shrinkage Cracking

Shrinkage is caused by the evaporation of water from the surface of fresh concrete and occurs when the surface drying rate is fast and the lost water cannot be replaced by bleed water. This moisture loss shrinks the concrete during the plastic stage and generates cracks. The shrinkage cracks begin as shallow cracks, but can become full-depth cracks later in the concrete’s life.

2.1.1.2 Settlement Cracking

Settlement cracks are caused by the tendency of concrete to consolidate after initial placement, vibration, and finishing. This consolidation, after fresh concrete is placed in contact with reinforcing steel or formwork, can locally restrain concrete deformation and generate cracks.

2.1.2 Cracking on Hardened Concrete

2.1.2.1 Drying Shrinkage

Drying shrinkage is one of the most important causes of hardened concrete cracking. It is generated by the loss of moisture from the cement paste, which shrinks its volume. The differential shrinkage between the surface and the interior concrete (or aggregates) causes tensile stress and generates cracks.

2.1.2.2 Thermal Stresses

Temperature gradients inside concrete structures can result in differential volume changes and generate cracks. The temperature gradients can originate from heat generated during the hydration process, or from weather conditions. When the local tensile stresses due to the differential volume changes exceed the local tensile strength of the material, the concrete will crack. Crack propagation is a matter for fracture mechanics, which will be discussed later in this chapter.

2.1.2.3 Chemical Reactions

Some materials used to make concrete or some chemical materials that penetrate into the material can generate harmful chemical reactions and cause cracking. In most cases, the chemical reactions cause the formation of a solid phase that occupies more volume than the original products from which it was formed, leading to the formation of cracks. The damages associated with alkali silica reaction and external sulfate attack fall into this category. (See relevant sections in this chapter and the chapter on Chemical Degradation.)

2.1.2.4 Freezing and Thawing

Freezing and thawing cycles lead to the formation of ice in concrete. Since ice occupies 9% more space than liquid water, internal stresses are generated. The formation of ice crystals starts in the larger pores. As space is filled, liquid pressure in the smaller pores increases. If air voids are present in the material, they will fill with water and contribute to reducing the tension in the material. Unsaturated pores will act similarly. However, if the material is near saturation and the volume and spacing of voids are inadequate, the concrete will sustain damage upon freezing and thawing.

2.1.2.5 Corrosion of Steel Reinforcement

Ingress of chloride ions can initiate corrosion of the reinforcing steel in concrete. The corrosion of steel generates products (various types of iron oxides) that occupy a volume greater than the original reinforcing bar. This increase in volume creates a high radial stress around reinforcing bars and results in cracks and subsequent concrete spalling (loss of thickness) and exposure of the reinforcing steel to the environment.

2.1.2.6 Poor Construction Practices

A wide variety of poor construction practices can result in the cracking of concrete structures. Foremost among these is the common practice of adding water to concrete to increase workability. Adding water has the effect of reducing strength, increasing settlement, and increasing drying shrinkage. When accompanied by a higher cement content to help offset the decrease in strength, an increase in water content will also mean an increase in the temperature differential between the interior and the exterior portion of the structure, resulting in increasing thermal stresses and cracking. In addition, by adding cementitious materials, even if the water to binder ratio (*w/b*) remains constant, more shrinkage will occur because the paste volume is increased.

Lack of curing will increase the degree of cracking within a concrete structure. The early termination of curing promotes shrinkage at a time when the concrete has low strength. The lack of hydration of the cement, due to drying, will result not only in

decreased long-term strength but also in the reduced durability of structures.

2.1.2.7 Construction Overloads

Construction loads can often be more severe than those experienced in service. Unfortunately, these conditions may occur at early ages when the concrete is most susceptible to damage, and they often result in permanent cracks. Precast members, such as beams and panels, are most frequently subject to this abuse. Cast-in-place concrete can also be affected.

2.1.2.8 Errors in Design and Detailing

Errors in design and detailing that may result in unacceptable cracking include use of poorly detailed re-entrant corners in walls, precast members, and slabs; improper selection or reinforcement detailing, or both; restraint of members subjected to volume changes caused by variations in temperature and moisture; lack of adequate contraction joints; and improper foundations design, resulting in differential movement within the structure.

2.1.2.9 Externally Applied Loads

It is well known that load-induced tensile stresses result in cracks in concrete structures. This point is readily acknowledged and accepted in the design of reinforced concrete structures.

2.2 Evaluation of Damage

Test methods for evaluation of damage in concrete structures are divided in two main groups: destructive and non-destructive. This section focuses on nondestructive methods and attempts to present some common methods described by ACI 228.2R-98. Some destructive methods such as coring, sampling, or measuring the in-situ strength of structures are not discussed in this section.

2.2.1 Visual Inspection

Visual inspection is one of the most versatile and powerful Non-Destructive Test (NDT) methods. However, its effectiveness depends on the knowledge and experience of the investigator. Visual inspection has the obvious limitation that only visible surfaces can be inspected. For these reasons, a visual inspection is usually supplemented by one or more of the other NDT methods discussed in this chapter.

2.2.2 Stress-Wave Methods

Several test methods based on stress-wave propagation can be used for nondestructive testing of concrete structures. The ultrasonic through-transmission method can be used for locating abnormal regions in a structure. The echo method can be used for thickness measurements and flaw detection. The spectral analysis of surface waves (SASW) method can be used to determine the thickness of pavements and elastic moduli of layered pavement systems.

2.2.3 Nuclear Methods

Nuclear methods can be subdivided into two groups: radiometric and radiographic. Both involve obtaining information about a test object due to interactions between high-energy electromagnetic radiation and the material.

2.2.4 Magnetic and Electrical Methods

These methods estimate where the corrosion of reinforcement is active. Corrosion activity can be monitored using the half-cell potential technique, and information on the rate of corrosion can be obtained from linear-polarization methods.

2.2.5 Penetrability Methods

Many of the degradation mechanisms in concrete involve the penetration of aggressive materials, such as sulfates, carbon dioxide, and chloride ions. As a result, concrete that has a surface zone that is highly resistant to the ingress of water will generally be more durable than concrete without such a resistive surface zone.

To assess the potential durability of in-place concrete, it is necessary to focus on methods that assess the ability of the surface zone to restrict the passage of external agents that may lead to direct deterioration of the concrete or to depassivation and corrosion of embedded reinforcement. Many test methods are based on the resistance of concrete to surface penetration. They can be grouped in three categories: water absorption (under a relatively low pressure head), water permeability (under higher pressure head), and air permeability.

2.2.6 Infrared Thermography

Infrared thermography has been used for detecting subsurface anomalies in concrete. Infrared thermography senses the emission of thermal radiation and produces a visual image from this thermal signal. Infrared thermography for testing concrete is based on two principles. The first principle is that a surface emits energy in the form of electromagnetic radiation. The second principle is that subsurface anomalies in concrete affect heat flow through concrete.

2.2.7 Radio Detection and Ranging (Radar) Method

This method is similar to the stress-wave method, discussed in Section 2.2.2, except that electromagnetic waves (radio waves or microwaves) are used instead of stress waves.

3.0 MODELING MECHANICAL DAMAGE IN CONCRETE

Materials are damaged when the combination of external and internal loads exceeds their elastic properties and ultimately lead to cracks and failure. The non-linear transition between elasticity and failure is associated with damage. Two different approaches are used to model damaged materials: damage mechanics and fracture analysis. Both approaches are reviewed in the next section.

Most damage analyses are based on the evaluation of crack system in the material. Yuan and Harrison (2006) reviewed different approaches for modeling damage. They introduced continuum damage mechanics and statistical approaches, also referred to in their paper as macroscopic and microscopic damage, respectively. The microscopic approach introduces a damage parameter that is the integration of crack volume over total volume (Kachanov 1993). The macroscopic approach uses a damage parameter to modify the elastic tensor that makes the connection between stress and strain in the material.

ACI (ACI MCP 2008 - 446.3R-97) also acknowledged these two dominant techniques used in finite element modeling of fracture in concrete. Yang and Chen (2003) presented smeared fractures as a damaged zone where an infinite number of small parallel cracks are distributed. In the damaged zone, crack propagation was simulated by reducing the material stiffness and strength. The constitutive laws were defined by nonlinear stress–strain relations with strain softening. The discrete crack model is based on displacement discontinuity, which is usually represented by nonlinear interface elements. In the following sections, macroscopic and microscopic damage approaches are discussed.

3.1 Damage Mechanics

The first step in damage analysis consists in defining a damage parameter for deriving a constitutive behavior law. This variable must be able to represent the state of degradation in the material in the damage phase. Carol and Bazant (1991) described damage using the concept of effective (or actual) stress. Figure 1 illustrates the concept of effective stress or real stress, which resists against loads in the undamaged zone. In this figure, σ and ε are stress and strain, respectively, σ' is the effective stress, which corresponds to undamaged part of material, and E is Young's modulus. According to Lemaitre and Chaboche (1985), the damage parameter is related to the cracked area divided by the total surface in a given direction:

$$d = \frac{A_0 - A}{A_0} = (1 - a) \tag{1}$$

where: A_0 and A are total and effective surface areas, respectively and a is a coefficient, which presents the undamaged surface (See Figure 1).

According to Equation (1), the damage parameter d can vary between 0 (undamaged) and 1 (fully damaged material).

One of the most common approaches for modeling mechanical damage in concrete was proposed by Mazars (Mazars and Pijaudier-Cabot 1989). The damage model is based on the positive part of the strain tensor. In the presence of large tensile and compressive stresses in concrete, damage is generated and propagated by tensile strain, which opens cracks. (The effect of compression strain is generally less than tensile strain because it closes cracks and does not generate damage.) In this approach, the elastic free energy of concrete ψ^e in a damaged condition can be written as a function of the tensorial form damage parameter $\underline{\underline{d}}$ and the elastic strain $\underline{\underline{\varepsilon}}^e$ (Chiarelli et al. and 2003 and Shao et al. 2004):

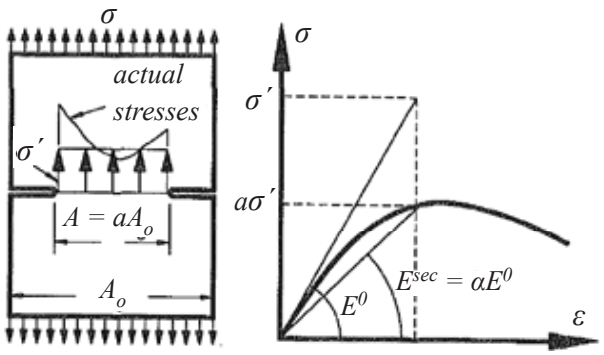

Figure 1. One Dimensional Damage Effect and Concept of Effective Stress (Carol and Bazant 1991)

$$\psi_e(\underline{\underline{\varepsilon}}^e, \underline{\underline{d}}) = \frac{1}{2}\lambda(tr\,\underline{\underline{\varepsilon}}^e)^2 + \mu\, tr(\underline{\underline{\varepsilon}}^e)^2 + \alpha\, tr\,\underline{\underline{\varepsilon}}^e tr(\underline{\underline{\varepsilon}}^e . \underline{\underline{d}}) + \beta\, tr\left[(\underline{\underline{\varepsilon}}^e)^2 . \underline{\underline{d}}\right] \tag{2}$$

where: α and β are the characteristic parameters, which describe the damage effects on an elastic material and can be obtained experimentally, and λ and μ are the Lamé coefficients, corresponding to the elastic parameters E (Young's modulus) and v (Poisson's ratio).

A description of Lamé coefficients is given in Equation (3):

$$\lambda = \frac{vE}{(1-2v)(1+v)} \qquad \mu = \frac{E}{2(1+v)} \tag{3}$$

A linear term depending on $\underline{\underline{\varepsilon}}^e$ can also be added to the free energy expression (Halm and Dragon 1998). This term allows damage-induced residual phenomena to be taken into account (residual or permanent strain after unloading $\sigma = 0$). In this case, the free energy is written as shown in Equation (4):

$$\psi_e(\underline{\underline{\varepsilon}}^e, \underline{\underline{d}}) = \frac{1}{2}\lambda(tr\,\underline{\underline{\varepsilon}}^e)^2 + \mu\, tr(\underline{\underline{\varepsilon}}^e)^2 + \alpha\, tr\,\underline{\underline{\varepsilon}}^e tr(\underline{\underline{\varepsilon}}^e . \underline{\underline{d}}) + \beta\, tr\left[(\underline{\underline{\varepsilon}}^e)^2 . \underline{\underline{d}}\right] + \gamma\, tr(\underline{\underline{\varepsilon}}^e . \underline{\underline{d}}) \tag{4}$$

where: γ is also a material parameter.

The corresponding stress equation is provided as Equation (5):

$$\underline{\underline{\sigma}} = \frac{\partial \psi_e}{\partial \underline{\underline{\varepsilon}}^e} = \lambda\, tr(\underline{\underline{\varepsilon}}^e)\underline{\underline{I}} + 2\mu\, \underline{\underline{\varepsilon}}^e + \alpha\left[tr(\underline{\underline{\varepsilon}}^e.\underline{\underline{d}})\underline{\underline{I}} + tr(\underline{\underline{\varepsilon}}^e).\ \underline{\underline{d}}\right] + \beta\left[\underline{\underline{\varepsilon}}^e.\underline{\underline{d}} + \underline{\underline{d}}.\underline{\underline{\varepsilon}}^e\right] + \gamma\underline{\underline{d}} \quad (5)$$

where: α, β and γ can be estimated from the results of a triaxial test (Shao et al. 2004 and Halm and Dragon 1998).

Chiarelli et al. (2003) introduced the following damage criterion:

$$f^d = \sqrt{\underline{\underline{\varepsilon}}^+ : \underline{\underline{\varepsilon}}^+} - (r_0 + r_1\, tr\, \underline{\underline{d}}) = 0 \quad (6)$$

where: $\underline{\underline{\varepsilon}}^+$ is the positive part of the strain tensor, and r_0 and r_1 are two characteristics of the material that can be estimated by a triaxial compression test. It is assumed that the evolution rate of the damage tensor has the same direction as the tensile strain tensor. (Halm and Dragon 1998).

The rate of damage evolution as a function of loading is described by Dragon et al. (2000):

$$\dot{\underline{\underline{d}}} = \dot{\lambda}_d \frac{\underline{\underline{\varepsilon}}^+}{\sqrt{\underline{\underline{\varepsilon}}^+ : \underline{\underline{\varepsilon}}^+}} \quad (7)$$

$$\rightarrow \begin{cases} \dot{\lambda}_d = 0 & \text{if} \quad f_d = 0 \ \ \& \ \ \dot{f}_d < 0 \\ \dot{\lambda}_d = \dfrac{\underline{\underline{\varepsilon}}^+ : \dot{\underline{\underline{\varepsilon}}}^+}{r_1\, tr\underline{\underline{\varepsilon}}^+} & \text{if not} \end{cases}$$

In some cases, the rate of damage is related to the crack volume propagation (Shao et al. 2004), to Young's modulus reduction (Lemaitre et al. 2000), or simply to the elastic strain rate (Jun et al. 2003). In this case, damage can be obtained arbitrarily from the elastic strain evolution in each direction:

$$\dot{\underline{\underline{d}}} = e\,\dot{\underline{\underline{\varepsilon}}}^e \quad (8)$$

where: e is a material characteristic.

3.2 Fracture Mechanics

Fracture mechanics is also referred to as crack propagation or crack growth, and is similar to damage. In both approaches, the appearance of cracks is due to excess loading that results in loss of cohesion between two continuous parts of the concrete structure. Contrary to the damage mechanics approach, the fracture mechanics predicts the geometry of the crack pattern in the material. This crack analysis can fully describe the state of concrete degradation and even give a homogenous damage analysis for the fractured zones (Mazars and Pijaudier-Cabot 1996).

Buyukozturk and Hearing (1998) analyzed crack propagation in concrete through and between material constituents. The development of bond cracks at the paste-aggregate interfaces is an important factor in inelastic deformation and in the fracture behavior of concrete. Bond cracks in normal strength concrete often propagate along the interface between paste and aggregates, absorbing energy before linking and forming continuous cracks through the paste at failure. Crack propagation produces a discontinuity in the material. One of the most common finite element techniques for modeling the discontinuity is an automatic remeshing. However, several methods also exist without the discontinuity model. Bouchard et al. (2003) compared three methods for crack propagation: the maximum circumferential stress criterion, the strain energy density fracture criterion, and the maximal strain energy release rate criterion.

3.2.1 Maximum Circumferential Stress Criterion (MCSC)

According to this criterion, crack propagation follows the direction of the maximum stress, which also corresponds to the direction of the maximum tensile stress. The approximation here is based on the fact that a crack propagates perpendicularly to the maximum tensile stress. It is a local approach since the direction of the crack growth is directly

determined by the local stress field along a small circle centered at the crack tip. The crack propagation then proceeds toward the integration point where maximum stress occurs (see Figure 2).

3.2.2 Minimum Strain Energy Density Criterion (MSEDC)

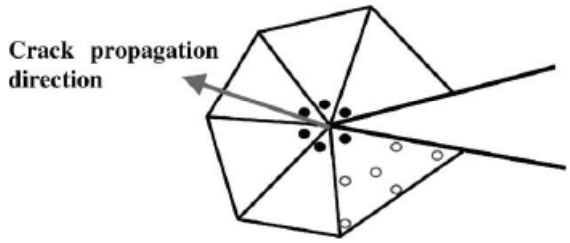

Figure 2. Crack Propagation Direction with Integration Points (Bouchard et al. 2003)

This method considers that high values of strain energy tend to prevent crack growth. Accordingly, the crack grows in the direction that minimizes this energy.

3.2.3 Maximum Strain Energy Release Rate Criterion (MSERRC)

The strain energy release rate represents the energy required to increase the crack length. The criterion is obtained when the strain energy release rate is maximal.

Comparisons showed that the MSEDC is less accurate than the two other criteria. The MCSC and MSERRC are equivalent in terms of accuracy and computation time. The MCSC appears to be the easiest to implement in any finite element code. However, it requires a refined mesh at the crack tip. The MSERRC is the most complex but gives good results. It requires a ring of elements around the crack tip, but its accuracy is mesh-independent (Bouchard et al. 2003).

3.3 Coupling between Damage and Transport Properties

Hydraulic and diffusion characteristics of concrete can be affected by damage. If concrete is damaged, the microcracks start to increase the porosity and/or connect isolated pores, which can raise the concrete's diffusivity or permeability. This report reviews relationships between damage propagation and hydraulic/diffusion characteristics of concrete.

Permeability of a single crack is often described by the simple Poiseuille flow equation (Snyder 2000, Gerard 1996). According to this theory, a crack is located between two infinite parallel plates. In this case, it is possible to show that:

$$K = \frac{w^2}{12} \tag{9}$$

where: K is the intrinsic concrete permeability and w is the crack's width.

Meschke and Grasberger (2003) present a refined expression for crack width by incorporating roughness and tortuosity effects:

$$w_h = \frac{w^2}{\tau_C^{2.5}} \tag{10}$$

In this equation, w_h is the equivalent crack width and τ_C is an empirical parameter, which describes the crack roughness. According to Meschke and Grasberger (2003), $\tau_C = 15$ can be taken into account for cracks in an ordinary concrete (OC).

Picandet et al. (2001) studied the evolution of gas permeability with damage in OC and HPC (high-performance concrete) and HPFC (high-performance steel fiber-reinforced concrete). They considered a simple scalar damage parameter via uniaxial compressive loading that accounted for the reduction of Young's modulus of elasticity. Their results showed that the evolution of gas permeability with damage can be modeled by an arbitrary exponential function:

$$\frac{K_{V(d)}}{K_{V(0)}} = exp(\kappa_1 d^{\kappa_2}) \quad (11)$$

in which $K_{V(0)}$ and $K_{V(d)}$ are initial and damaged gas permeabilities, respectively, d is the damage parameter and κ_1 and κ_2 are two experimental parameters.

Other studies focused on the effect of damage on diffusion coefficient. The diffusion coefficient of typical undamaged OC is about 10^{-12} m²/s (Gerard et al. 1998). This coefficient increases until maximum damage is reached for a completely cracked material. In this case, the diffusion coefficient tends to the free water diffusion value, which is about 10^{-9} m²/s. Gerard et al. (1998) presented the following relationship to take into account the changes in diffusion properties as a function of damage:

$$D_d = D_0 + D_{max}\left[1 - \frac{1}{1+\left(\frac{d}{d_{cr}}\right)^n}\right] \quad (12)$$

where: D_d, D_0 and D_{max} are the damaged, initial undamaged, and maximum (for completely cracked material) diffusion coefficients, respectively, d is the damage parameter, and n and d_{cr} are model parameters ($n = 5$ and $d_{cr} = 0.4$).

According to Gerard et al. (1998), D_{max} can be estimated as 80% of the free water diffusion coefficient.

This approach was further refined by Gerard and Marchand (2000) using the double porosity concept. From a microscopic approach based on a crack opening, they found:

$$D_d = \frac{D_{max} + SD_0}{1+S} \quad (13)$$

where: S is the ratio of the surface perpendicular to the diffusion flow of uncracked concrete, divided by the surface of cracked concrete, and can be calculated as:

$$S = \frac{1-d}{d} \quad (14)$$

where: d is the damage parameter, presented by Equation (1).

4.0 EARLY-AGE CONCRETE DAMAGE

Early-age cracking is one of the major problems of concrete structures because it can potentially affect the durability of the structures. Fresh concrete analysis requires a thermo-hydro-chemical model coupled to mechanical equations. Rapid evolution of mechanical resistance, drying shrinkage, and heat of hydration are some of the problems related to fresh concrete. Heat of hydration, particularly in mass volume concrete structures, can be detrimental to the durability by generating cracks and consequently reducing the service life. Similarly, high moisture gradients during curing can induce drying shrinkage and cracks. The objective of this section is to explain the mechanical characteristics of early-age concrete and related damage models.

4.1 Degree of Hydration

One of the most important parameters for analyzing early-age concrete is estimating its degree of hydration. The degree of hydration is a time dependent variable which defines the hydration progress from the first contact of cement and water to fully hydrated cement paste. Hua et al. (1995) used this parameter to estimate the amount of shrinkage strain. They presented the degree of hydration as a ratio of bonded water at time t to total consumed water for full hydration:

$$\xi = \frac{W_t}{W_\infty} \quad (15)$$

where: ξ is the degree of hydration, W_t and W_∞ are the quantities of consumed water at time t and for full hydration respectively. W_∞ can be estimated according to the cement type and W_t is determined by the weight difference between the specimen dried at 105°C and heated to 1,050°C.

Ulm and Coussy (1998) developed this concept and presented the rate of hydration in an Arrhenius form:

$$\dot{\xi} = A_H \, exp\left(-\frac{E_a}{RT}\right) \tag{16}$$

where: $\dot{\xi}$ is the rate of hydration, E_a is the activation energy, R is the gas constant, T is the temperature, and A_H can be considered as a normalized affinity.

4.2 Evolution of Mechanical Characteristics

Mechanical characteristics of early-age concrete change with time. ACI (ACI 209R-92) provides expressions, based on experimental results, to estimate the compressive strength and Young's modulus of concrete with time. Equations (17) and (18) provide expressions for compressive strength and Young's modulus as a function of time during concrete hydration.

$$(f'_c)_t = \frac{t}{\alpha_f + \beta_f t}(f')_{28} \tag{17}$$

where: $(f'_c)_t$ is the compressive strength at time t, $(f'_c)_{28}$ is 28-day compressive strength and α_f and β_f are two constants.

$$E_t = g_{ct}\left[w_c^3 (f'_c)_t\right]^{1/2} \tag{18}$$

where: E_t is Young's modulus at time t, w_c is the specific weight of concrete (kg/m³), $(f'_c)t$ is the time dependent compressive strength (MPa), and g_{ct} is a constant (0.043, according to ACI 209R-92).

4.3 Shrinkage

According to the definition of ACI, shrinkage is the strain measured on a load-free concrete specimen as a result of induced capillary forces occurring during drying (ACI 209.1R-05). When concrete shrinks with time due to the evaporation of moisture, stress develops if the concrete member is fixed to other structural components, thereby causing cracks. Generated cracks have adverse effects on the service life and durability of the structure. Shrinkage depends on the environment condition (especially the relative humidity), the concrete mixture and the size of the specimen and does not include length changes due to temperature variations. Shrinkage strain is usually measured by casting companion load-free specimens identical to the loaded concrete specimens used to measure the total strain. Typical shrinkage values are given by ACI (ACI 209.1R-05) as dimensionless strains. Long-term concrete shrinkage values are typically between 200 and 800×10^{-6} mm/mm. Mortar shrinkage values are typically between 800 and $2{,}000\times10^{-6}$ mm/mm. Cement paste shrinkage values are typically between 2,000 and $6{,}000\times10^{-6}$ mm/mm.

ACI separates the shrinkage strain in two main groups:

- **Autogenous shrinkage -** The shrinkage occurring during the absence of moisture exchange (as in sealed concrete specimens), due to the hydration reactions taking place inside the cement matrix, is defined as autogenous shrinkage. Autogenous shrinkage is usually small for many normal compressive strength concretes and can usually be neglected. For concrete with water-cement ratios (w/c) less than 0.40, however, autogenous shrinkage may be a significant component of the total measured shrinkage (ACI 209.1R-05).
- **Drying shrinkage -** Shrinkage occurring in a specimen that is exposed to drying condition is called drying shrinkage. For normal-strength

concrete, it is usually assumed that the entire shrinkage strain is due to drying shrinkage, and any contribution from autogenous shrinkage is neglected. Final value of drying shrinkage can be estimated by its relation to water loss of concrete.

Figure 3 illustrates these two types of shrinkage strain and compares their intensity, time of initiation and evolution with time with other sources of strain.

Some factors that affect the drying shrinkage are: concrete quantity, characteristics, size of aggregates, water/cement ratio, size and shape of the specimens (see Equation (19) and relative humidity of environment (see Equation (20). Experimental measurements made on drying shrinkage are very sensitive to the dimensions, shape of the specimens, and boundary conditions (Benboudjema et al. 2005).

4.3.1 Size Effect on the Shrinkage Strain

The ACI associates the shrinkage strain to the shape of specimen with the following expression:

$$\varepsilon^{sh} \propto \frac{1}{\left(V/S\right)^2} \tag{19}$$

where: V is the volume of specimen and S is its drying surface area.

4.3.2 Relative Humidity or Water Loss Effect on the Shrinkage Strain

The ACI relates the shrinkage strain to the relative humidity by the following expression:

$$\varepsilon^{sh} \propto 1 - \left(\frac{RH\%}{100}\right)^b \tag{20}$$

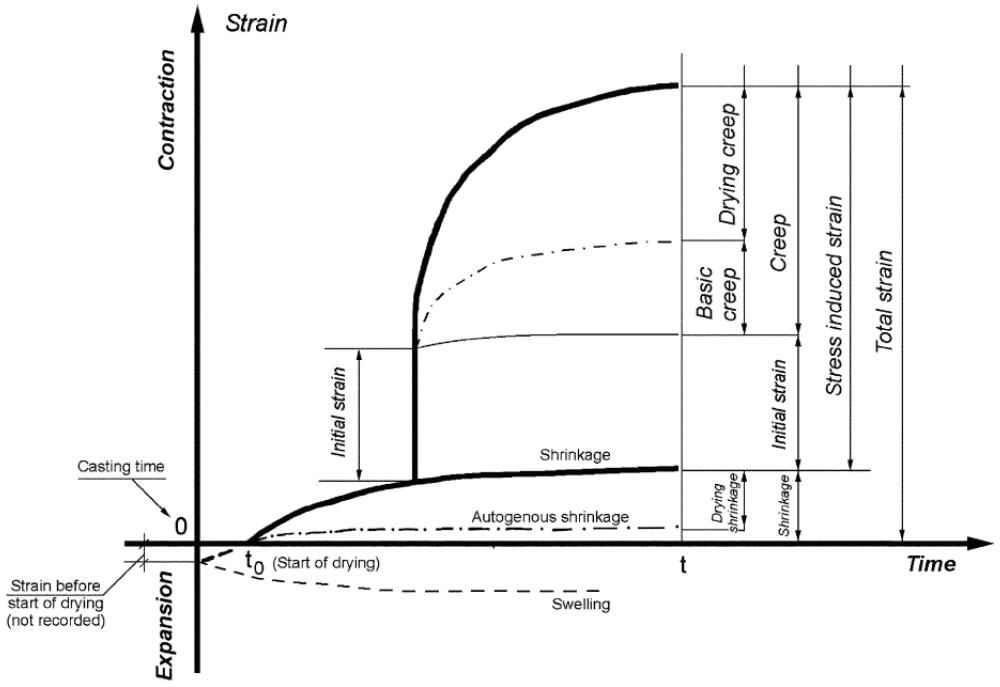

Figure 3. Evolution of Various Strains as A Function of Time (ACI 209.1R-05)

where: ε^{sh} is shrinkage strain, *RH* is the relative humidity in percent and *b* is a parameter that ranges from 1 to 4.

Rahman et al. (2000), by studying repaired concrete structures, proposed a linear relationship between the moisture loss and the free shrinkage strain:

$$(\Delta\varepsilon^{sh})_t = G(\Delta W_l)(\varepsilon^{sh})_u \tag{21}$$

where: $(\Delta\varepsilon^{sh})_t$ is an increment in free shrinkage strain at time *t*, $(\varepsilon^{sh})_u$ is the ultimate free shrinkage strain and $G(\Delta W_l)$ is an experimentally determined function that allows the mapping from moisture loss ΔW_l to the free shrinkage strain.

Benboudjema et al. (2005) also reproduced experimental results, highlighting that drying shrinkage strains are proportional to moisture loss. They proposed the following relationship:

$$\dot{\varepsilon}^{sh} = k_{ds}\dot{W}_c I \tag{22}$$

where: $\dot{\varepsilon}^{sh}$ is the rate of drying shrinkage strain, $\dot{W}_c$ is the rate of water content evolution, k_{ds} is the hydrous compressibility factor, and *I* is the unit tensor.

Bazant (2001) summarized various aspects for the predicting concrete shrinkage and presented two prediction models to estimate the shrinkage strain. One model is an approximate prediction formula for pore relative humidity distributions, and is required for realistic creep and shrinkage analysis. The other deals with the extrapolation of short time measurements of creep and shrinkage to long times.

The first approach can be written as:

$$= \frac{(\varepsilon^{sh})_t}{(\varepsilon^{sh})_u} = \frac{W_c^0 - W_c^t}{W_c^0 - W_c^\infty} \tag{23}$$

where: W_c^0 is the initial specific evaporable water content in concrete, W_c^t is the average specific water content, and W_c^∞ is the final water loss.

The second approach is written as:

$$(\varepsilon^{sh})_{t+1} = P_6(\varepsilon^{sh})_t \tag{24}$$

where: $(\varepsilon^{sh})_{t+1}$ is the new value of shrinkage strain obtained from the previous time step value $(\varepsilon^{sh})_t$, and P_6 is defined as:

$$P_6 = \frac{\sum_i (\varepsilon^{sh})_t (\bar{\varepsilon}^{sh})}{\sum_i (\varepsilon^{sh})_t^{\,2}} \tag{25}$$

where: $\bar{\varepsilon}^{sh}$ and $(\varepsilon^{sh})_t$ are measured and estimated values of shrinkage strain respectively for the previous time steps and subscript *i* deals with the number of known data points.

4.3.3 Total Shrinkage Strain

According to ACI committee 209 (ACI 209R-92), total axial shrinkage strain varies with time and approaches its ultimate value. It can be predicted using the following formulas:

$$(\varepsilon^{sh})_t = \frac{t}{35+t}(\varepsilon^{sh})_u \quad \text{Shrinkage after curing for 7 days for moist cured concrete}$$

$$(\varepsilon^{sh})_t = \frac{t}{55+t}(\varepsilon^{sh})_u \quad \text{Shrinkage after curing for 1–3 days for steam cured concrete} \tag{26}$$

where: $(\varepsilon^{sh})_u$ is the ultimate shrinkage strain ($\approx 800\times10^{-6}$ for moist cured and $\approx 730\times10^{-6}$ for steam cured, according to ACI-209 for an ordinary concrete).

The calculated shrinkage strains using ACI equations can be transformed into initial strain loads or equivalent temperature gradients using Equation (27):

$$\varepsilon^{sh} \approx \varepsilon^T = \alpha_T \,.\, \Delta T \Rightarrow \Delta T = \varepsilon^{sh} / \alpha_T \tag{27}$$

where: ε^T is the thermal strain, α_T is the concrete thermal expansion coefficient. Using this analogy, the thermal coefficient must be calibrated to fit the shrinkage strains.

4.3.4 Preventing Shrinkage

There are various methods for controlling of shrinkage cracking. Good curing practice can decrease considerably the shrinkage. Control joints, shrinkage strips, and shrinkage compensating concrete are some typical methods referred by ACI (ACI 224R-01). Rongbing and Jian (2005) also described a chemical process called ethoxylation to synthesize a shrinkage-reducing admixture.

4.4 Heat of Hydration

When cement is mixed with water, the exothermic chemical reactions of the hydration process generate heat. The heat generated by the cement's hydration raises the temperature of concrete. To model the heat of hydration, Cervera et al. (Cervera 1999, Cervera 1999b) added a source term f_ξ to the energy conservation equation. This term models the heat generated by the chemical reactions when the cement is mixed with water:

$$f_\xi = Q_\xi \dot{\xi} \tag{28}$$

where: Q_ξ is a material constant and ξ is the degree of hydration.

They present a rate of hydration, $\dot{\xi}$, in Equation (29), which has a different form than that in Equations (15) and (16):

$$\dot{\xi} = \frac{n_1}{n_0}\left(\frac{A_\xi}{n_1\xi_\infty} + \xi\right)(\xi_\infty - \xi) \times exp\left(-\frac{n_2\xi}{\xi_\infty}\right) exp\left(-\frac{E_a}{RT}\right) \tag{29}$$

where: A_ξ is the initial affinity of the hydration reaction, ξ_∞ is the maximum degree of hydration, E_a is the activation energy of the hydration process, R is the ideal gas constant, and T is the temperature. The other parameters, i.e., n_0, n_1, and n_2 are material constants to be determined experimentally.

The hydration process can be coupled with the mechanical model by adding a component to the total strain equation (30), called the hydration strain ε^H, which is the contribution from the self-generated heat of cement's hydration. This strain is proportional to the hydration degree:

$$\varepsilon^H = \alpha_T^\xi \, \xi \, I \tag{30}$$

where: α_T^ξ is the thermal expansion parameter associated to the heat of hydration and I is the unit tensor.

Similar models considering the hydration process were described in (Ulm and Coussy, 1995 and 1998, and Gawin et al. 2006).

4.5 Damage Model

Several models have been proposed in order to study the early-age behavior of concrete structures by means of finite element calculations. Calculations are performed by considering phenomena related to fresh concrete characteristics such as thermal expansion from the hydration process, shrinkage strain, chemical strain, etc. Gawin et al. (2006) presented a rheological behavior model according to the following equation:

$$\varepsilon = \varepsilon^e + \varepsilon^c + \varepsilon^T + \varepsilon^o \tag{31}$$

where: ε^e is elastic strain, ε^c is creep strain (sum of visco-elastic and viscous flow strain), ε^T is thermal strain, and ε^o is autogenous strain.

In this approach, drying shrinkage is assumed to be a part of the elastic strain ε^e. (Elastic strain is the sum of drying strain plus strain caused by external loading.) Moreover, the rate of shrinkage strain is modeled as a function of relative humidity evolution. Also, autogenous strain, according to this approach, is supposed to be equivalent to the chemical strain as a function of hydration degree.

Ulm and Coussy (1995) presented another model in which total strain is equal to the sum of elastic, thermal, and chemical strain.

$$\varepsilon = \varepsilon^e + \varepsilon^T + \varepsilon^{sh} \quad (32)$$

where: ε^{sh} is shrinkage strain which contains autogenous and drying shrinkage. Globally, chemical strain is modeled as a function of hydration degree.

To obtain the expression of elastic strain, the mechanical behavior of fresh concrete can be modeled. Benboudjema and Torrenti (2008) presented an elastic damage model coupled to shrinkage as follow:

$$\dot{\sigma}' = C^t_\xi \dot{\varepsilon}^e \quad (33)$$

where: $\dot{\sigma}'$ is the rate of effective stress, C^t_ξ is the fourth order elasticity stiffness tensor and $\dot{\varepsilon}^e$ is the rate of elastic strain.

The elastic strain, depending on the type of rheological model, can be obtained. Equations (31) and (32) are two examples of such models. C_ξ can be obtained knowing Young's modulus and Poisson's ratio. In this approach, Poisson's ratio is supposed to be constant and Young's modulus can be calculated by an equation similar to Equation (18). Finally, the effective stress can be obtained from the total stress σ and the damage parameter d:

$$\sigma' = \sigma (1-d) \quad (34)$$

The damage parameter can be calculated by a damage model such as Equation 7). It is important to mention that, in this approach, the elasticity stiffness tensor is considered independent of the damage parameters (different from Equation 5) and the elasticity stiffness tensor varies only as a function of hydration (Young's modulus evolution).

5.0 SULFATE ATTACK

5.1 Introduction

There are two main theories that attempt to explain the cause of expansion of cement-based specimens subject to sulfate ingression:

- Paste expansion hypothesis and
- Crystal growth pressure hypothesis.

Both hypotheses attempt to explain the formation of gaps around aggregates in concrete as seen in some experiments (Taylor et al. 2001). The gaps may have been caused by stress generated from the growth of ettringite crystals (crystal growth hypothesis) or from the expansion of cement paste due to the formation of fine ettringite crystals in the cement paste prior to the formation of bigger crystals in the gaps (Shimada et al. 2005).

The crystal growth pressure hypothesis suggests that the growth of large ettringite crystals around the aggregates in concrete generates pressure and leads to expansion followed by cracking. From thermodynamic considerations, it was shown that nucleation of ettringite crystals will occur preferentially at crack tips (Shimada et al. 2005 and Tixier and Mobasher 2003b) which results in stress concentration at the crack tips. If this stress is high enough, micro-cracks can form, propagate and coalesce to form macro-cracks and ultimately spalling and failure.

The paste expansion hypothesis suggests that expansion of the paste leads to formation of gaps around the aggregates. Ettringite recrystallizes in those gaps and results in cracking (Taylor et al. 2001). Due to the heterogeneous nature of the cement paste, cracks are expected to occur in the paste region also.

The preferential location of ettringite formation has also been debated. The two schools of thought are:

- Racks are generated by the stress due to nucleation of ettringite crystals present in the crack tips (Fu et al. 1994) and
- Cracks are caused by the stress generated by the compact crystals present in the pores.

These two theories present competing explanations and accepting either one of them needs more evidence. A brief description of different issues is given by Stark and Bollman (1999). An interesting insight about the factors affecting crystallization in pores can be found in (Scherer 1999).

5.2 Numerical Modeling of Damage Due to Sulfate Attack

As mentioned earlier, there is no consensus among researchers regarding the mechanism of sulfate attack. Thus, numerical simulation of the phenomenon is only possible if a fairly conservative approach is taken based on simplified assumptions. Figure 4 depicts a general algorithm used to model sulfate attack, as reviewed in the next sections. When sulfate penetrates a cement-based structure, it reacts with some of the cement hydration products and forms ettringite. As the volume of ettringite is greater than the reactants, it induces strain on the surrounding cement matrix. The strain leads to stress, which results in cracking when the stress exceeds the strength of the material. The presence of cracks increases the diffusivity of sulfate in the material. This results in ingression of more sulfates and the cycle is repeated until the structure fails.

Several numerical models have been developed to numerically simulate the phenomenon of sulfate attack and are listed below:

- Atkinson and Hearne (1989) developed one of the earliest models for sulfate attack of cementitious materials. This model was based on an empirical relation between volumetric expansion of the structure and the total amount of ettringite formed. The correlation between the volume of ettringite formed and the overall expansion observed was established and based on some experimental data.
- Ping and Beaudoin (1992) developed a model based on chemical-thermodynamic principles. This model assumed that the expansion resulted from the conversion of chemical energy in the form of crystallization pressure to mechanical energy, which was sufficient to overcome the cohesion of the system.
- Krajcinovic et al. (1992) developed a simple micromechanical model based on homogenization

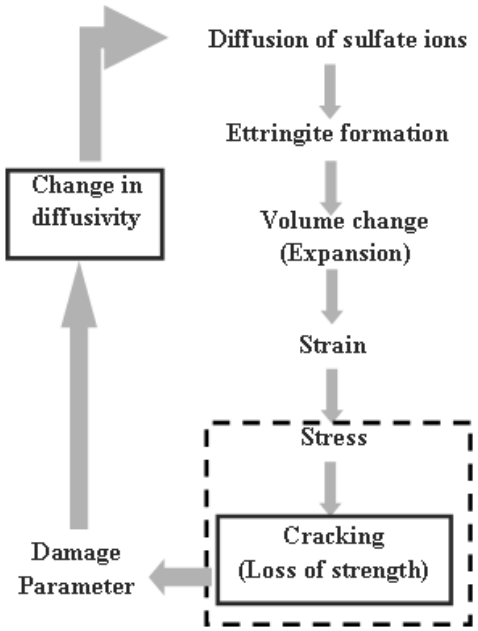

Figure 4. Global Approach for Modeling Sulfate Attack Degradation of Cementitious Materials

of microscopic responses on a macro scale for evaluation of macro response of the structure. This model has been refined recently (Basista and Weglewski 2008).

- Clifton and Pommersheim (1994) developed a model on the assumption that volume change in the reaction expands the paste, which is linearly dependent on the amount of ettringite formed (following Atkinson and Hearne 1989).
- Gospodinov et al. (1996) developed a model, which includes diffusion of chemical species into cement and its effects (e.g., filling up voids). This model did not include the effects of cracking on the material parameters.
- Saetta et al. 1998 developed a general framework for the evaluation of mechanical behavior under physical/chemical attacks. This model evaluated the coupled effects of moisture, heat and chemical species. Evaluation of expansion and cracking due to chemical attacks was not included in the model.
- Schmidt-Dohl and Rostasy (1999) developed another general model which was based on thermodynamics and kinetics considerations for evaluating degradation of structures under chemical attacks. This model can only be used for species with known thermodynamic data. Also, comparison of the mechanical parameters obtained from this model with experimental data posed considerable difficulty.
- Samson and Marchand et al. (Marchand 2001, Marchand et al. 2002, Samson and Marchand 1999, Samson et al. 1999a, 1999b and 1999c and Samson et al. 2003) developed a numerical model for describing the mechanism of ionic transport in unsaturated cement systems. It included ionic diffusion, moisture transport, and chemical reactions in the use of the extended Nernst-Planck equation and it incorporated the effects of micro-structural changes, with a considerable degree of detail, on the transport properties of chemical species in the cementitious materials. But this model did not consider the changes in mechanical properties and their effects on transport properties.
- Tixier and Mobasher (2003) developed a model similar to the one developed by Clifton and Pommersheim (1994) with a different analytical expression assumed for expansion.
- Shazali et al. (2006) developed a general model to evaluate the degradation of concrete under sulfate attack but only in relation to gypsum formation. Damage was quantified by a chemical damage parameter (similar to Saetta et al. 1998) and was incorporated to evaluate the strength of the specimen.

Tixier's (Texier and Mobasher 2003a) and Krajcinovic-Basista's model (Krajcinovic et al. 1992 and Basista and Weglewski 2008) are discussed in more detail because these two models attempted to include the effects of chemical reactions on mechanical properties and the effects of structural damage (e.g., cracking) on the hydraulic properties of structures.

5.2.1 Tixier's Model

The purpose of the model is to simulate the response of cement-based structures exposed to external sulfate attack. The changes in the material properties and the hydraulic properties are evaluated using a macro-scale damage, represented by the damage parameter d in Equation (1).

In this model, three calcium aluminate phases (e.g., calcium monosulfate, unreacted tricalcium aluminate and tetracalcium aluminate hydrate) are assumed to react with sulfate ions and produce ettringite. The equivalent reaction is given as[1]

$$C_{\text{av}} + q\overline{S} \rightarrow C_6A\overline{S}H_{32} \tag{35}$$

[1]Cement Notation: C = CaO; S = SiO_2; A = Al_2O_3; F = Fe_2O_3; $\overline{S}$ = SO_3; $\overline{C}$ = CO_2; K = K_2O; N = Na_2O; M = MgO; H = H_2O

where: C_{av} is the average weight of the concentrations of tetracalcium aluminate hydrate, monosulfate and residual tricalcium aluminate and q is an equivalent stoichiometric coefficient of the lumped reaction expressed as:

$$q = 3\frac{UC_3A}{N} + 2\frac{MMono}{N} + 3\frac{MTAH}{N} \quad (36)$$

UC_3A is the molar concentration of unreacted tricalcium aluminate, *MMono* is the molar concentration of calcium monosulfate, *MTAH* is the molar concentration of the tetracalcium aluminate hydrate, and N is the total molar concentration of the three reactants.

5.2.1.1 Diffusion and Chemical Reactions

The coupled diffusion and chemical reaction processes using Fick's law of diffusion without convection and a second order reaction as expressed below:

$$\frac{\partial U}{\partial t} = D\frac{\partial^2 U}{\partial X^2} - kUC_{av} \quad (37)$$

$$\frac{\partial C_{av}}{\partial t} = -\frac{kUC_{av}}{q} \quad (38)$$

where: U is the concentration of sulfate, C_{av} is the lumped concentration of calcium aluminate, D is the effective diffusivity of sulfate ions through the cement-based system, k is the reaction rate constant, q is defined as in Equation (36), and t is the time.

5.2.1.2 Strain Development

Stress within a representative volume element is calculated based on the net change in volume of the reaction products relative to the reactants (∇V_s). If (∇V_s) > 0, volumetric strain per representative unit volume of the structure is calculated as:

$$\bar{\varepsilon} = \frac{\Delta V_s}{V} \quad (39)$$

where: V is the initial volume. Assuming a porosity fraction b is available for deposition of solid products, the net strain is computed as:

$$\varepsilon' = \bar{\varepsilon} - b\varphi \quad (40)$$

Assuming that the material is isotropic, uniaxial strain is calculated as:

$$\varepsilon = \frac{\varepsilon'}{3} \quad (41)$$

5.2.1.3 Stress-Strain Relations

Subsequently, experimentally determined stress-strain diagram is used to relate the calculated strain from chemical reaction due to volumetric expansion to stress, crack formation and a damage parameter, d. An example stress-strain diagram for cementitious materials under tensile stress is shown in Figure 5.

Cementitious materials contain pores and micro-cracks, which do not affect the strength of the structure in the elastic range (segment *OA* in Figure 5). In the nonlinear phase (segment *AB* in Figure 5), new micro-cracks will form, which will finally coalesce to *B* to form macro-cracks leading the structure to fail as defined by the nonlinear descending curve.

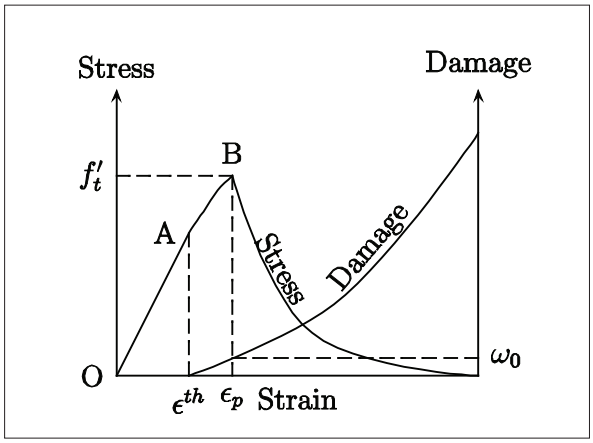

Figure 5. Stress Strain Diagram of Concrete Under Tension

In the nonlinear ascending phase of stress strain diagram, an equivalent Young's modulus (E^*) can be expressed as:

$$E^* = E(1–d) \tag{42}$$

where: E is the Young's modulus obtained as the initial tangent or the slope of the linear part of the curve (segment *OA* in Figure 5).

For the uniaxial case, stress σ, and strain ε in the nonlinear phase are related as:

$$\sigma = E(1–d)\varepsilon \tag{43}$$

Assuming that the damage parameter is not affected by the Poisson's ratio of the damaged structure, d can be expressed as (Karihaloo 1995 and Budiansky and O'Connell 1976):

$$d \approx \frac{16}{9} k' \left(1 - \frac{\varepsilon^{th}}{\varepsilon}\right)^m \tag{44}$$

where: ε^{th} is the threshold strain at which micro-cracks start forming and k' and m are calibration parameters. The parameters are calibrated by combining Eqs. (43)-(44) and using an experimental stress-strain diagram.

The post-peak response of the structure (segment BC in Figure 5) is modeled by using a relation proposed by Nemat-Nasser and Hori in 1993 (Tixier and Mobasher 2003a) given as:

$$\frac{\sigma}{f_t'} = \sqrt{\frac{\tan(\pi\omega_0 / 2)}{\tan(\pi\omega / 2)}} \tag{45}$$

where: σ is the stress, f_t' is the maximum tensile stress, and ω_o is the damage parameter corresponding to the peak stress.

The unloading is assumed to be elastic and the elastic modulus in the post-peak region is obtained by

$$E^* = \frac{\sigma}{\varepsilon - \varepsilon_0} \tag{46}$$

where: $\varepsilon_0 = \varepsilon_p - \frac{f_t'}{E_0}$, ε_p is the strain at the maximum tensile stress.

Average expansion is expressed as (Tixier and Mobasher 2003a)

$$\Delta = \sigma_r \left(\frac{1}{\bar{E}} - \frac{1}{E_0}\right) L \tag{47}$$

where: $\bar{E}$ is the average Young's modulus over the cross section, L is the gauge length of the specimen and σ_r is the residual strength which can be viewed as a scaling factor.

5.2.1.4 Change in Diffusivity

A linear relationship between the damage parameter and diffusivity is assumed in this work and is expressed as

$$D(d) = d(D_1 - D_2) + D_2 \tag{48}$$

where: D_1 Is the effective diffusivity of sulfate ions through cracked structure and D_2 is the effective diffusivity of sulfate ions through the uncracked structure.

5.2.2 Krajcinovic-Basista's Model

The Krajcinovic-Basista's model incorporates coupled physico-chemical processes of non-steady diffusion with chemical reaction, topochemical reaction[2] of ettringite formation, expansion of

[2] "A reversible or irreversible reaction that involves the introduction of a guest species into a host structure and that results in significant structural modifications to the host..." (IUPAC 1997).

ettringite crystals, formation of micro-cracks and evolution to macro-cracks. This is a unique attempt to capture the behavior at the micro and macro-scales and the transition across these scales. For this model, the diffusion process and the second order chemical reaction are evaluated the same way as in Tixier's model (see (41) and (42)) but the diffusivity of sulfate in uncracked cement-based structure is calculated from (Garboczi and Bentz 1992):

$$\frac{D_i}{D_i^{\mu}} = 0.001 + 0.07\varphi_{cap}^2 \cdot + 1.8H(\varphi_{cap} - 0.18)(\varphi_{cap} - 0.18)^2 \quad (49)$$

where: D_i^{μ} is the diffusivity in the free solution and φ_{cap} is the fraction of capillary porosity.

Also, the expansive strain due to ettringite formation in this model is calculated similar to the way in Tixier's model (Tixier and Mobasher 2003).

5.2.2.1 Calculation of Damage Parameter

The damage parameter is used to bridge micro-scale and macro-scale responses. In the micro-scale, the growing ettringite crystal exerts pressure on the surrounding cement paste matrix. If the stress exceeds the fracture toughness of the cement paste matrix, micro-cracks start to propagate and finally coalesce to form macro-cracks.

Assuming that a small notch exists at the matrix-inclusion interface, the stress intensity factor can be approximately calculated as

$$K_I = \frac{2p^n}{\sqrt{\pi a_c}}\left(a_c - \sqrt{a_c^2 - r_{a0}^2}\right) \quad (50)$$

where: p^n is the swelling pressure, r_{ao} is the initial radius of the calcium aluminate particle and a_c is the mean half crack length of penny shaped cracks.

The terminal half crack length at the completion of reaction by a single C_3A particle can be approximately calculated using the fracture toughness K_{IC} of the cement paste. The damage parameter, ω, is then calculated using the following equation (Budiansky and O'Connell 1976):

$$\omega = N_a a_c^3 \quad (51)$$

where: N_a is the number of particles of C_3A consumed (equivalent to the number of cracks if assumed to be under mean field effects) and a_c is the half crack length.

5.2.2.2 Stress-Strain Relations

The relation between stress and strain at the macro scale is given as

$$\varepsilon = S(\omega) : \sigma + \varepsilon^I \quad (52)$$

where: σ is the stress at macro scale, $S(\omega)$ is the compliance matrix which reflects the degradation in material properties through ω and

$$\varepsilon^I = f^I \varepsilon^{**} \quad (53)$$

where: f^I is the inclusion volume density and ε^{**} is the eigenstrain.

The compatibility condition in one dimension is expressed as

$$\frac{d^2}{dx^2}[\sigma(x,t) + E(x,t) f^I(x,t)\varepsilon^{**}(x,t)] = 0 \quad (54)$$

For the case of no external traction on the structure, the expansion is given as

$$\varepsilon = \frac{1}{E(x,t)}\int \varepsilon^{**}(x,t)E(x,t)f^I(x,t)dx = f^I(x,t)\varepsilon^{**}(x,t) \quad (55)$$

where: ω_c is the conduction percolation threshold at which a spanning cluster traverses and joins with another spanning cluster.

Its value is obtained as 0.182 from the results of numerical simulation by Charlaix in 1986 (Basista and Weglewski 2008).

5.2.2.3 Change in Material Properties

The effects of cracking on the mechanical as well as hydraulic properties of the structure are related to the damage parameter. Change in effective diffusivity through the structure due to crack formation in the mean field regime, when cracks are dilute in concentration allowing assumption of a homogeneous structure under the influence of average stresses, is defined as:

$$D = D_0(1+\frac{32}{9}\omega) \tag{56}$$

following a model developed by Salganik (1973).

where: D_0 is the diffusivity in the uncracked cement-based structure and ω is the damage parameter. Young's modulus and Poisson's ratio are obtained from the damage parameter using the following relations (Budiansky and O'Connell 1976):

$$E = E_0(1-\frac{16}{9}\omega) \tag{57}$$

$$\nu = \nu_0(1-\frac{16}{9}\omega) \tag{58}$$

where: the subscript $''0''$ denotes the uncracked matrix and the non-subscripted parameters denote cracked matrix.

A scaling law is used to describe diffusion in the percolation regime, where micro-cracks coalesce to form a macro-crack, following numerical simulations by Stauffer in 1985 (Krajcinovic et al. 1992): (59)

$$D_p \propto (\omega-\omega_c)^{\mu_\omega} \tag{59}$$

where: $\mu_\omega \approx 2$ is a universal exponent for a three-dimensional case.

The modified diffusion coefficient is now given as

$$D = D_0(1+\frac{32}{9}\omega)+D_p \tag{60}$$

where: $D_p = D_0\frac{(\omega-\omega_c)^2}{(\omega_{ec}-\omega)}$ for $\omega_c < \omega < \omega_{ec}$. ω_c is the conduction percolation threshold as mentioned before and ω_{ec} is the elastic or rigidity percolation threshold at which a cluster of cracks transects the volume.

The stiffness of the structure beyond the elastic percolation threshold is essentially zero. In the crossover regime from conduction percolation threshold to elastic percolation threshold the variations of elastic moduli need more investigation. From a self-consistent estimation, the rigidity percolation threshold comes out to be 9/16 which is 0.8 times the value of the threshold obtained through numerical simulation by Sornette (Krajcinovic et al. 1992). Krajcinovic et al. (1992) suggested, assuming the percolation threshold to be 9/16, that the elastic moduli can be assumed to be linearly dependent on the damage parameter in the percolation regime. Basista and Weglewski (2008) suggested that the linear relation in the percolation regime is probably not a good approximation but rather that this regime needs to be modeled using percolation theory. However, the biggest challenges in doing so are (1) translation of the damage parameter obtained from the mean field regime to an equivalent porous structure and then (2) translating the response of the structure back to an equivalent damage parameter that will reflect the damaged state on the macro-response of the structure.

6.0 CORROSION-INDUCED CRACKING

Reinforcement corrosion is one of the most important problems affecting the durability of concrete structures. When steel reinforcement corrodes, the chemical reaction produces corrosion products that occupy more volume than the original steel. This creates a pressure on the concrete cover (Dekoster et al. 2003, Bhargava et al. 2006) and hoop or tangential tension around the rebar. The radial component of this pressure increases with the corrosion product expansion. Cracking occurs when the tangential component or hoop stress exceeds the maximum tensile strength of concrete. The crack propagates from the steel-concrete interface to the surface of the concrete. Crack propagation analysis can give a criterion for an estimate of the structure's durability or service life.

This report focuses only on the mechanical aspect of the corrosion problem. The corrosion process is initiated by the ingress of chloride and carbonation. These topics are covered in the chemical degradation report.

6.1 Corrosion Mechanism

The mechanism of corrosion using an analytical calculation base for a single reinforcement was described by Liu and Weyers (1998). They introduced a simple model that can estimate the time needed for producing a crack in the concrete cover.

Figure 6 shows the three phases of damage propagation. On the figure, R_s is the initial radius of the steel bar, c is the thickness of the concrete cover layer, d_0 is the width of the high porosity interfacial concrete zone, R_i is R_s plus d_0, R_0 is R_i plus c, d_1 is the radius of steel lost by corrosion, P_r.is the pressure induced by the corrosion product, d_c is the deformation under this pressure, and R_c is the radius of the damaged zone. In phase (I), corrosion starts. In phases (II), corrosion consumes a portion of the steel bar, fills the porous zone and starts to apply pressure on the concrete cover. Finally, in phase (III), tangential component or hoop stress of radial pressure P_r damages the surrounding zone.

The embedded reinforcement is usually surrounded by a ring of concrete having a high porosity. When corrosion starts, the process consumes steel. The

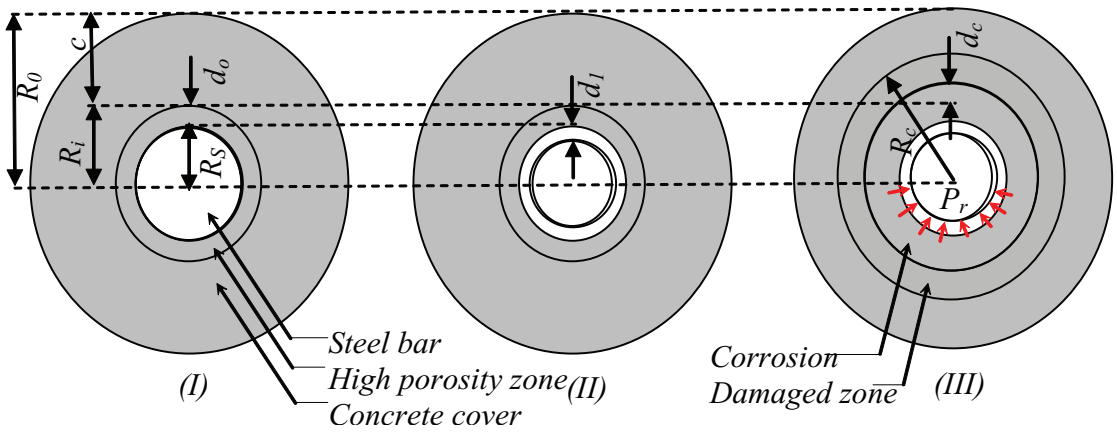

Figure 6. Rust Propagation and Induced Pressure After Bhargava et al. (2006)

corrosion products, which occupy more volume than the original steel, fill this porous zone easily. It is assumed that filling this zone does not change the stress around the reinforcement. So, the initial radius of the reinforcement system, R_i, is considered equal to the initial radius of the steel bar, R_s, in the high porous concrete zone d_0 (Figure 6).The distance d_1 in Figure 1 shows the radius of steel lost by corrosion. When d_0 is filled completely, more corrosion product creates a pressure P_r. It is assumed that this pressure is uniform on the external face of the reinforcement, inside of the corroded zone and on the internal face of the concrete cover in contact with the corroded zone. This pressure is applied to the concrete and induces a deformation as shown by d_c in Figure 6. This imposed deformation creates a damaged zone with radius R_c. Bhargava et al. (2006) described an analytical method that estimates the necessary time that R_c can reach R_0, corresponding to a completely damaged concrete cover.

A similar description was proposed by Wang and Liu (2006).

6.2 Corrosion Expansion

One of the most important steps in corrosion modeling is the estimation of the expansion caused by the formation of corrosion products. Empirical relationships have been proposed to model the imposed displacement by corrosion products around the reinforcement.

Dekoster et al. (2003) proposed that the expansion thickness equals two times the initial thickness. Du et al. (2006) described the crack propagation in concrete cover in four steps:

- Internal cracking due to radial expansion and tangential tension, which creates the first crack inside the concrete cover;
- Before the internal cracks penetrate the concrete cover, external cracks appear on the surface of the material;
- Penetration cracking when outside cracks reach inside cracks and;
- Ultimate cracking of concrete under tensile stress decreases the resistance and increases the softening until no further development of cracks occurs.

Du et al. (2006) proposed typical values of radial expansion of 0.005, 0.0012, 0.0015, and 0.0017mm for internal, external, penetration, and ultimate cracking, respectively, for a rebar with 8mm diameter and 8mm concrete cover.

Wang and Liu (2006) used a linear function between the volume of accumulated corrosion product ΔV_C and the original volume of reinforcement V_R:

$$\Delta V_C = n_V \ \Delta V_R \tag{61}$$

where: n_V is the ratio of the rust volume on initial steel volume and varies between 1.7 and 6.15 according to different corrosion products.

Bhargava et al. (2006) used an equation, which relates the mass density change of corrosion products to their chemical formula:

$$\rho_r = \frac{\rho_s}{\alpha_1 \alpha_2} \tag{62}$$

where: ρ_r and ρ_s are mass densities of corrosion products and original steel respectively, and α_1 and α_2 are two coefficients, which depend on the type of corrosion product. They proposed the values for these two coefficients (Table 1).

6.3 Rate of Corrosion

Wang and Liu (2006) proposed a corrosion propagation time that is a function of the bar radius, concrete cover thickness and annual mean corrosion current density. The corrosion current density is also discussed by Ahmad (2003). It is related to the corrosion rate by:

Table 1 . Coefficient α_1 and α_2 for Different Types of Rust Production in Concrete

Corrosion Products	FeO	Fe_3O_4	Fe_2O_3	$Fe(OH)_2$	$Fe(OH)_3$	$Fe(OH)_3{\cdot}3H_2O$
α_1	0.777	0.724	0.699	0.622	0.523	0.347
α_2	1.80	2.00	2.20	3.75	4.20	6.40

$$J_r = \left(\frac{W}{F}\right) I_{cor.} \tag{63}$$

where: J_r is the instantaneous corrosion production rate, W is the equivalent weight of steel, F is Faraday's constant and $I_{cor.}$ is the corrosion current density that is measured on steel bar.

Martin-Pérez (1999) presents a similar procedure for computing J_r using the ionic valence of the iron ion and equivalent molar weight of corrosion products. The proposed relationship is written as:

$$J_r = \left(\frac{W}{z m_{Fe} F}\right) I_{cor.} \tag{64}$$

where: z is the ionic valence of ferric iron and equals 2 according to the following equation:

$$Fe \rightarrow Fe^{2+} + 2e^{-} \tag{65}$$

and m_{Fe} is the number of moles of iron needed to produce one mole of corrosion product.

It is equal to 3 for the case of magnetite formation according to the following equation:

$$3Fe + 2O_2 \rightarrow Fe_3O_4 \tag{66}$$

where: W is the molar mass of corrosion product, equals to 231.14 g/mol for magnetite.

Assuming a homogenous distribution, the mass of the corrosion product can be calculated as:

$$m_r = 2 J_r (\Delta t) \pi R_s \tag{67}$$

where: m_r is the mass of the corrosion product, R_s is the reinforcement radius and Δt is the elapsed time.

The total expansion volume of corrosion product, ΔV_c, can be calculated according to Martin-Pérez (1999):

$$\Delta V_C = m_r \left(\frac{1}{\rho_r} - \frac{\alpha}{\rho_s}\right) \tag{68}$$

This gives a displacement equal to (see Figure 6):

$$d_c = \frac{\Delta V_C}{2\pi R_s} \tag{69}$$

This displacement, d_c, is the thickness of corrosion products on the rebar as a function of time. It can be imposed homogenously around the reinforcement for to model the mechanical effect of the corrosion process.

6.4 Modeling the Damage Induced by Corrosion

Most models found in the literature are based on semi-analytical approaches that estimate the time to cracking from a simple mechanical analysis. Two such models were reviewed. Another model based on a coupled multiphysic analysis was also reviewed and presented at the end of this chapter.

6.4.1 Liu and Weyers' Model (1998)

According to the definition, the critical mass of corrosion products is the mass that fills the porous area surrounding the reinforcement and sets pressure on concrete cover until crack production and failure.

This critical mass calculated in Liu and Weyers' approach is the sum of two terms:

- Mass of rust for filling the porous zone that can be obtained according to Figure 6 using:

$$M_P = 2\pi \rho_r R_s d_0 \tag{70}$$

where: M_P is the mass of corrosion products needed to fill the porous ring around the reinforcement, and ρ_r is the density of the corrosion products.

- Mass of new corrosion products that form after the porous zone is filled. These new corrosion products apply pressure on the concrete cover and generate a stress greater than the tensile strength of concrete. The mass per unit rebar length of these additional corrosion products is given by:

$$M_S = \rho_r \left(2\pi (R_s + d_0) d_c + \frac{M_{st}}{\rho_s} \right) \tag{71}$$

where: M_S is the mass of the corrosion products required to produce a cracked zone with thickness equal to d_c the thickness of corrosion. M_{st} and ρ_s are steel bar mass consumed and steel mass density, respectively.

The critical corrosion product mass is thus given by the sum of Equations (70) and (71), after neglecting the term $d_o d_c$ as being very small:

$$M_{crit} = \rho_r \left(2\pi R_s (d_0 + d_c) + \frac{M_{st}}{\rho_s} \right) \tag{72}$$

The stress-strain relationship, for a concrete cover with thickness C around the reinforcement (see Figure 6), can be estimated analytically in a cylindrical coordinate system (Timoshenko and Goodier 1970).

Assuming that the formation of corrosion products corresponds to an imposed displacement d_c, the pressure on the concrete shell around the rebar is given by:

$$P_r = \frac{E_{ef} d_c}{(R_s + d_0)(m_C + \nu)} \tag{73}$$

where: ν is the Poisson's ratio and E_{ef} is the effective Young's modulus, given by:

$$E_{ef} = \frac{E}{1 + \theta} \tag{74}$$

where: E is Young's modulus of the undamaged concrete and θ equals to the creep coefficient.

The parameter m_c is given by:

$$m_C = \frac{((R_s + c)^2 + R_s^{\,2})}{((R_s + c)^2 - R_s^{\,2})} \tag{75}$$

By supposing a thick-wall concrete cylinder around the reinforcement with a linear stress distribution from the inside surface of concrete cover to the outside and assuming that, at the failure limit, the outside stress is equal to the tensile strength of concrete, pressure can be calculated as:

$$P_r = \frac{c f_t}{R_s} \tag{76}$$

in which f_t is the tensile strength of concrete.

Combining Equation (76) with Equation (73) yields an expression for d_c, the concrete deformation due to the formation of corrosion products.

$$d_c = \frac{c f_t}{E_{ef}} (m_C + \nu) \tag{77}$$

Equations (62) and (77) can be replaced in Equation (72) to find the critical corrosion mass products.

$$M_{crit} = \frac{2\pi\rho_r \rho_s R_s}{\rho_s - \alpha_1 \rho_s}\left(\frac{c\, f_t}{E_{ef}}(m_C + \nu) + d_0\right) \quad (78)$$

Liu and Weyers (1998) presented the corrosion product formation rate as a function of time t as the following equation:

$$\frac{dm_r}{dt} = \frac{\kappa_C}{m_r} \quad (79)$$

The coefficient κ_C is the rust production rate and is defined as (Thoft-Christensen 2000):

$$\kappa_C = 0.766 \times 10^{-3}\, R_s\, i_{cor} \quad (80)$$

where: i_{cor} is the mean annual corrosion rate, obtained from experimental measurements.

The time to initiate concrete cover cracking can be calculated by integrating Equation (79):

$$t = M^2_{crit} / 2\kappa_C \quad (81)$$

6.4.2 Martin-Pérez's Model (1999)

Martin-Pérez (1999) assumed a concrete cover formed by a cracked and an uncracked layer (see Figure 7). The analytical solution for the tangential stress, under an imposed pressure P_r at the boundary of the cracked zone (with radius R_c) can be written as:

$$\sigma^t = \frac{R_s R_c R_r}{(c + R_s)^2 - R_c^2}\left(1 + \frac{(c + R_s)^2}{R_c^2}\right) \quad (82)$$

In this equation, P_r is the pressure at the steel/concrete interface.

The pressure distribution inside the concrete cover is given by (see Figure 7):

$$P_C = P_r \frac{R_s}{R_c} \quad (83)$$

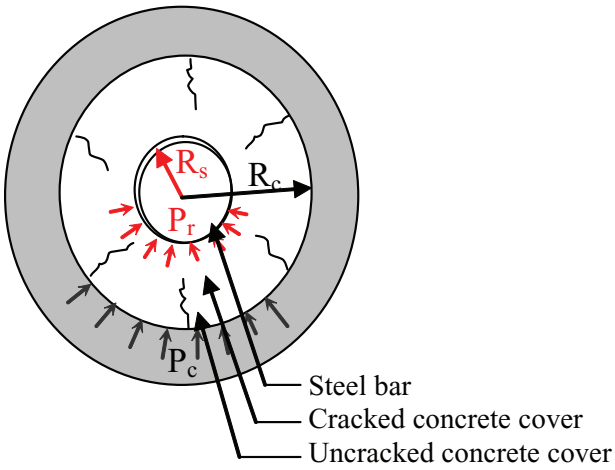

Figure 7: Pressure Distribution Around the Reinforcement

It is assumed that an internal crack occurs when the tangential stress, given by Equation (82), exceeds the concrete tensile strength.

By considering Equations (80) and (81), a value of R_c for which the tangential stress is maximum can be found. This is illustrated by drawing the ratio of P_r/σ_t as a function of R_C. Figure 8 shows this curve for a steel rebar of 16-mm diameter and a 20-mm concrete cover.

This figure shows that, for a small R_c value (radius of damaged zone, see Figure 7), the P_C value is high but c is large; inversely for a large amount of R_c, P_C is smaller but c is decreased. The optimal value of R_c can be found by calculating the derivative P_r/σ_t with respect to R_c, which gives:

$$R_r^{Max} = 0.486\,(c + R_s) \quad (84)$$

Substituting R_c^{Max} in Equation (82) and replacing the tangential stress with the tensile strength of concrete f_t gives the maximum internal pressure that can be sustained by the concrete cover before cracking:

$$P_r^{Max} = f_t \frac{\left(\frac{c}{2R_s}\right) + 0.5}{1.665} \quad (85)$$

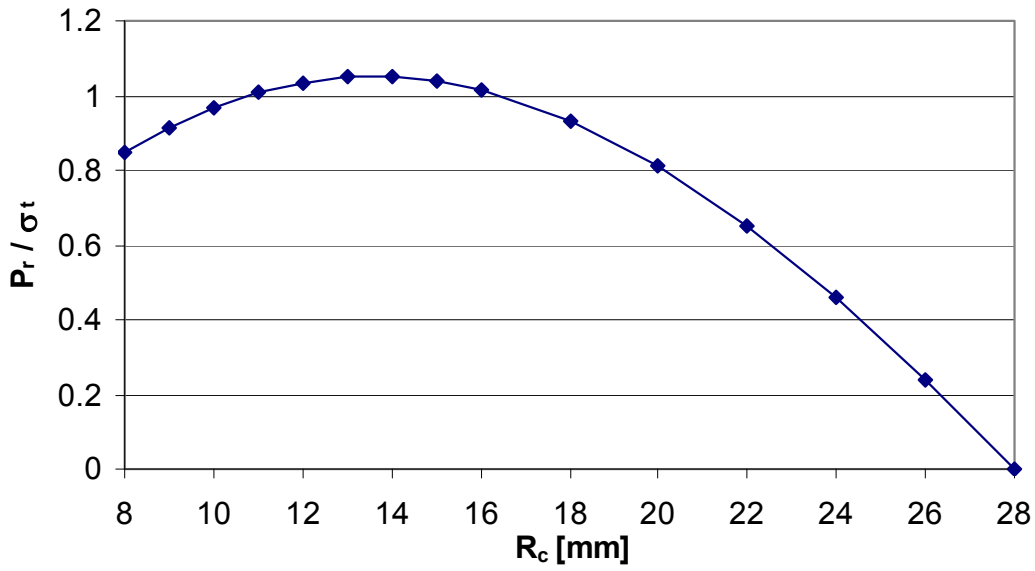

Figure 8. Maximum Pressure Resistance of Concrete Cover as A Function of Radius

This calculated P_c^{Max} value corresponds to the strain imposed by the corrosion expansion:

$$\varepsilon_v = \frac{2P_r^{Max}}{E_r}(1+\nu_r)(1-2\nu_r) \tag{86}$$

where: ε_v is the dilatation (volumetric strain) and E_r and ν_r are Young's modulus and Poisson ratio of rust production, respectively.

E_r is related to the bulk modulus of rust:

$$E_r = 3(1-2\nu r)K_r \tag{87}$$

The values $\nu_r = 0.499$ and $K_r = 2$ GPa were used by Martin-Pérez.

The expansion volume of concrete can be calculated from the dilatation:

$$\Delta V_C = \varepsilon_v \; V \tag{88}$$

where: V is the initial volume of steel; it gives the mass of rust production:

$$M_{crit} = \Delta V_C /(\frac{1}{\rho_r} - \frac{\alpha_1}{\rho_s}) \tag{89}$$

The corresponding time for the production of the critical mass of corrosion products (mass necessary to initiate cracking), based on Equation (67), is given by:

$$t = M_{crit} /(2\pi R_s J_r) \tag{90}$$

where: J_r was defined by Equation (63).

6.5 Numerical Simulation of Corrosion Damage

Beside the semi-analytical models studied, concrete cracking by corrosion can also be modeled by numerical methods. Numerical models are particularly useful for complicated reinforcement geometries. The implementation of such model in a numerical code allows taking into account several multi-physics phenomena that play an important part in the estimation of the service life of materials. Chen and Mahadevan (2008) presented a numerical model of concrete cracking due to corrosion, coupled with heat transfer and chloride penetration. They compared the crack propagation patterns in concrete structures using both a constant and a dynamic corrosion rate, as a function of the chloride content.

Equation (91) presents the corrosion current model used by Chen and Mahadevan, based on experimental data from (Liu and Weyers 1998):

$$I_{cor} = 0.926 . \exp\left[7.98 + 0.7771 \ \ln(1.69 C_t) - \frac{3006}{T} - 0.00011 R_r + 2.24 t^{-0.215} \right] \quad (91)$$

where: I_{cor} is the corrosion current density, C_t is the total chloride content, T is temperature, t is corrosion time, and R_r is the ohmic resistance of the concrete cover. R_r is also related by an empirical regression relationship to the total chloride content:

$$R_r = \exp\left[8.03 - 0.549 \ln\left(1 + 1.69 C_t\right) \right] \quad (92)$$

Figure 9 shows the radial displacement on the concrete–steel interface, obtained by two methods.

To model cover cracking, Chen and Mahadevan (2008) applied a linear elastic model for the tension part of the stress and a perfectly plastic model for the compression part for which the ascending part follows the Desayi and Krishnan model with the following expression:

$$\sigma = \frac{E\varepsilon}{1 + \left(E\varepsilon / 2 f_c' \right)} \quad (93)$$

where: σ and ε are stress and strain, respectively, E is the Young's modulus and (f_c') is the ultimate compressive strength. Application of the numerical code allows using a more sophisticated mechanical model to analyze cracking and damage propagation.

7.0 ALKALI-SILICATE REACTION

Alkali-silica reaction (ASR) is one of the most important causes of concrete structural damage. ASR has been observed on many different types of structures including dams, pavements, and bridges. Ever since its discovery in 1940 by Stanton (Stanton 1940), many studies have been conducted to describe the mechanisms of ASR and how various parameters affect the expansion of aggregates and the production of cracking. But this phenomenon remains unclear and research is still ongoing.

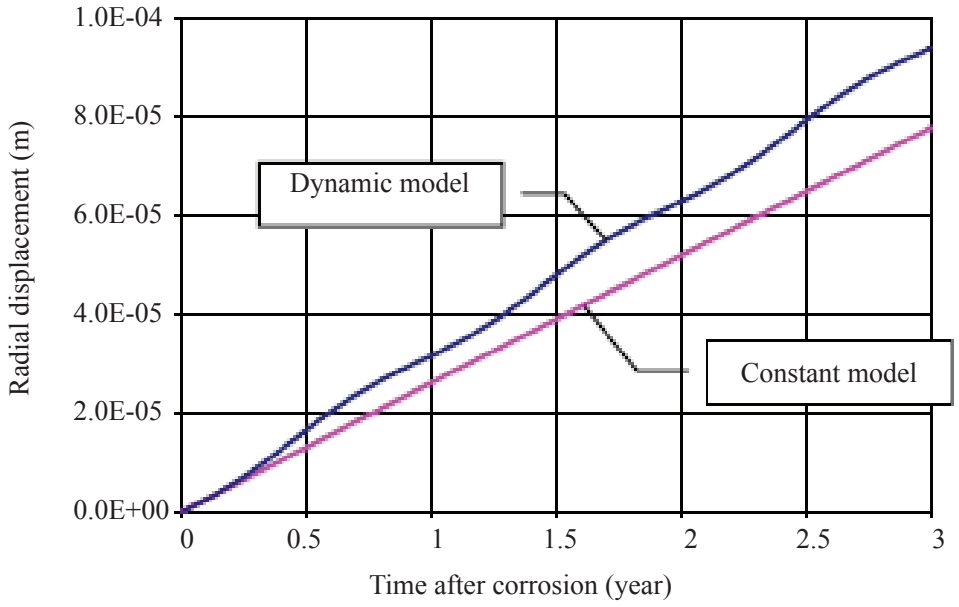

Figure 9 . Variation of the Radial Displacement Versus Time (Chen and Mahadevan 2008)

7.1 Mechanisms of ASR

It is generally agreed that the three essential components for the ASR in concrete structures are the presence of: (1) reactive silica (from aggregates), (2) sufficient alkalis (mainly from Portland cement, but also from other sources, internal or external, of concrete), and (3) sufficient moisture.

The term "reactive silica" refers to aggregates that tend to react with the alkali hydroxides (sodium and potassium) to form ASR gel. It is important to note that not all siliceous aggregate can be the source of ASR. The inherent reactivity of aggregates depends on several factors including; mineralogy, degree of crystallinity, and solubility of the silica in pore solution. Aggregates susceptible to ASR must also contain a certain amount of reactive minerals such as opal, tridymite, cristobalite, and volcanic glass.

The composition of the ASR gel is not well understood. It is commonly accepted that the expansion is induced by the formation of a hydrous alkali silicate gel, which forms as the result of reactions between the silicate aggregates and alkali hydroxide ions in the hydrated cement paste matrix pore solution (Glasser 1992, Diamond 2000). The composition of this gel is still a topic of discussion (Knudsen and Thaulow 1975, Diamond 2000).

Over the past decades, many researchers have considered ASR gel to be a mixture of several components containing various proportions of alkali, calcium, and silicate (Powers and Steinour 1955, Scrivener and Monteiro 1994, Helmuth and Stark 1992). Helmuth and Stark (1992), referring to the equilibrium phase results of Kalousek (1944), concluded that the gel could be entirely expressed as a combination of an alkali silicate hydrate (ASH) phase and a calcium alkali silicate hydrate phase. More recent data from X-ray diffraction (XRD) analyses, Si nuclear magnetic resonance (NMR) spectroscopy and molecular dynamic (MD) modeling, suggest that the structure of natural and synthetic ASR gels could be rather similar to kanemite ($NaHSiO_2O_5$-$3H_2O$) (Weiker et al. 1996, Hou et al. 2004, Kirkpatrick et al. 2005). NMR spectroscopy data also demonstrated that the ASR gel could only be formed in chemical environments of low calcium and high silicate concentrations (in solution). In concrete, these conditions can be obtained by the formation of a reactive transport barrier around the aggregates.

7.2 ASR Test Methods

The ASR related test methods, according to Figure 10, can be divided into laboratory and in-situ tests.

Laboratory tests are also divided into two main categories: tests on concrete and tests on aggregates. ASTM C 227 covers the determination of the susceptibility of cement-aggregates combination to expansive reaction with ASR by measuring the increase or decrease in length of a specimen during storage under prescribed test conditions. ASTM C 1293 allows estimating the ASR potential of aggregates with pozzolan or slag. ASTM C1260 and C 1567 can be used with more aggressive conditions, which permit detection of ASR potential within 16 days. Finally, ASTM 289 is the laboratory test that covers chemical determination of the potential reactivity of aggregates by storing crushed and sieved aggregates in sodium hydroxide solution.

In situ tests are generally divided in two main groups: destructive test (DT) and non-destructive test (NDT) methods. Destructive tests mainly consist in in-situ coring. Cored samples can then be analyzed according to the laboratory tests mentioned previously. Some common NDT methods for the assessment of condition of ASR-affected structures are Spectral Analysis of Surface Waves (SASW), related Multiple Impact Surface Waves (MASW) methods, Impact Echo (IE) using patented Impact Echo Scanner, and Slab Impulse Response (SIR). The objective of all in-situ NDT tests is to locate damaged zones affected by ASR.

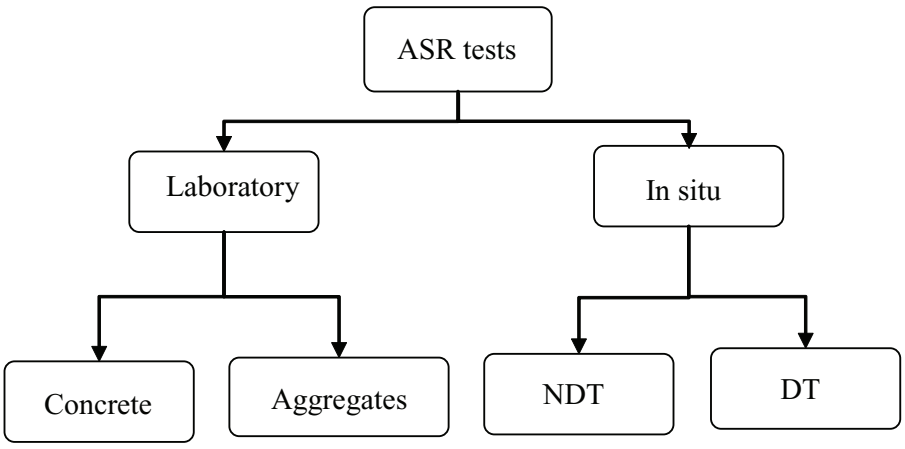

Figure 10. ASR Test Methods

7.3 ASR Mitigation

It is well-known that concrete expansion due to ASR can be suppressed by the addition of pozzolanic material (Chatterji 2005). The required quantity of supplementary cementitious materials is primarily a function of aggregate type and mixture characteristics (Thomas 1996, Fournier and Bérubé 2000, Duchesne and Bérubé 2000, Thomas et al. 2006). The benefits of lithium-based admixtures for ASR mitigation are also well documented (Folliard et al. 2003, Tremblay et al. 2004, Millard and Kurtis 2008). Lithium can be used to suppress the expansion arising from most reactive aggregates (Thomas et al. 2006). Finally, it is well known that restricting the alkali contribution of the portland cement component and reducing the internal relative humidity in concretes below a certain value can be effective for controlling the ASR expansion. The maximum tolerated alkali content (that associated with the expansion limit that produces damage) and critical relative humidity are both related to the reactive aggregate type (Bérubé et al. 2002a, Fournier and Bérubé 2000, Multon et al. 2008). The use of coatings and sealants to reduce the internal relative humidity of concrete can also mitigate ASR in bridge decks and pavements (Bérubé et al. 2002a).

7.4 Modeling of Damage Induced by ASR

Over the years, several theories have been proposed to explain the volume instability of concrete affected by ASR. Some have attempted to describe the swelling mechanisms at the pore scale. In most of these approaches, the expansion of concrete is induced by the swelling of the amorphous silica gel, which eventually cracks the material. According to one of the most prevalent views, the change in volume of concrete is due to the hydrophilic nature of the gel, which tends to absorb water by osmosis. While absorbing water, the gel swells and locally creates internal pressures (Dent-Glasser and Kataoka 1981, Diamond et al. 1981). More recently, the expansion of concrete by the alkali-silica reaction was attributed to surface phenomena. This theory assumes that the interaction of the gel with the ionic species present in the pore solution of hydrated cement pastes generates electrical double layer repulsive forces, whose intensity is determined by the composition and the ionic strength of the surrounding electrolyte (Prezzi et al. 1997, Prezzi et al. 1998). ASR production has a high sensitivity to temperature and externally applied stresses (Multon and Toutlemonde 2006).

The progressive expansion of concrete by ASR can be described by continuum mechanic models. According to these approaches, concrete swelling is the result of the interaction between the expanding gel, the pore fluid, and the concrete skeleton (Li and Coussy 2002, Ulm et al. 2002). All these phenomena are described at the material scale.

ASR modeling at the microscopic scale is complicated because the chemical reactions are not well known and the phenomenon is not distributed homogenously. Capra and Sellier (2003) presented a probabilistic approach, which considered the ASR as a homogenous function of temperature and humidity in materials and calculated the orthotropic swelling of concrete due to gel formation. In this approach, ASR swelling is considered as one contribution of the total strain:

$$\varepsilon_i = \varepsilon_i^e + \varepsilon_i^{pl} + \varepsilon_i^{ASR} \tag{94}$$

in which index i refers to direction, and ε, ε^e, ε^{pl} and ε^{ASR} are total, elastic, plastic and ASR-associated strain, respectively.

Inelastic strain due to ASR is modeled as a function of ASR cracking probability, Pf^{ASR}, in the direction i:

$$\varepsilon_i^{ASR} = \alpha_\varepsilon \frac{Pf_i^{ASR}}{1 - Pf_i^{ASR}} \tag{95}$$

where: α_ε is a material constant to be determined.

In this approach, the damage coefficient is presented under tensile (d^t) or compressive (d^c) conditions. The damage expression for tensile stress in direction i is a function of cracking probabilities Pf, and is expressed as:

$$d_i^t = 1 - (1 - Pf_i^t)(1 - Pf_i^c)(1 - Pf_i^{ASR}) \tag{96}$$

where: subscripts c and t refer to compression and tension.

The damage parameter has the same definition as in Section 3.1. Each probability of cracking, Pf, can be calculated on the basis of a Weibull distribution (Equation 97):

$$Pf_i^{ASR} = 1 - exp\left(-\frac{1}{m^{ASR}} \left(\frac{\langle \sigma_i - \sigma_{gi} \rangle^+}{\sigma_i^{ur}} \right)^{m^{ASR}} \right)$$

$$Pf_i^t = 1 - exp\left(-\frac{1}{m^t} \left(\frac{\langle \sigma_i \rangle^+}{\sigma_i^{ut}} \right)^{m^t} \right) \tag{97}$$

$$Pf_i^c = 1 - exp\left(-\frac{1}{m^c} \left(\frac{\left\langle \sigma_i + \sqrt{(C)^2((\langle \sigma_j \rangle^-)^2 + (\langle \sigma_k \rangle^-)^2} \right\rangle^+}{\sigma_i^{uc}} \right)^{m^c} \right)$$

where: the function $\langle x \rangle^+$ equals zero when x is negative and equals x when x is positive, m and σ^u are the Weibull's law parameters, σ_i is the stress in direction i, σ_j and σ_k are stresses perpendicular to i, C is the coefficient of variation and σ_{gi} is the stress induced in undamaged material in direction i.

In the case of ASR cracking, $\sigma_g i$ is related to the gel pressure, P_g:

$$\sigma_{gi} = \frac{P_g}{(1 - Pf_i^{ASR})} \tag{98}$$

The relation between σ_{gi} and P_g is shown in Figure 11 (Capra and Sellier 2003 and Li et al. 2000). According to this figure, the total stress σ is equal to (Li et al. 2000):

$$\sigma = \sigma_{gi} - P_g \tag{99}$$

This concept is illustrated by the rhelogical model demonstrated in Figure 12 (Li and Coussy 2002):

The pressure induced by the gel, as a function of time t, can be written as:

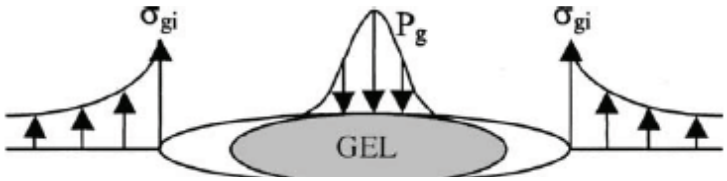

Figure 11. Stress and Pressure Induced by ASR Gel in Equilibrium

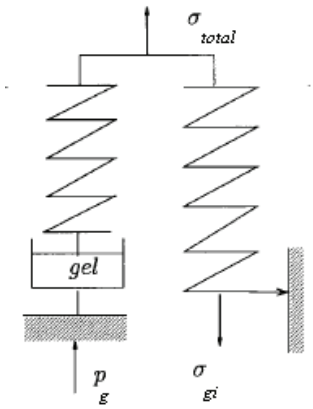

Figure 12. Rhelogical Model of One-dimensional Chemoplastic Material

$$P_g(t) = K_g \left\langle \frac{P_{g\,\lim}(t)}{1 + P_{g\,\lim}(t)(\kappa_e \mathrm{tr}\varepsilon + \kappa_p \phi_0)} \right\rangle^{+} \quad (100)$$

where: tr ε is the volumetric strain, ϕ_0 is the initial porosity, K_g is the gel stiffness and κ_e and κ_p are two constants related to crack and porosity respectively.

The parameter $P_{g\,lim}\,(t)$ can be calculated as a function of relative humidity *RH* and temperature *T* by Equation (101).

$$P_{g\,lim}(t) = P^{\infty}_{g\,lim}\, RH^{\,m_{RH}} \times \left(1 - \exp\left(-k_0 \exp\left(\frac{-E_a}{RT}\right) t\right)\right) \quad (101)$$

where: E_a is the activation energy of the ASR reaction, R is the gas constant, k_0 is a characteristic of the chemical process and m_{RH} is a parameter that reduces the impact of RH on pressure ($m_{RH} = 8$). $P^{\infty}_{g\,lim}$ is the maximum gel pressure in a totally saturated condition. According to the work of Larive (referred by Li et al. 2000), this value of maximum gel pressure, $P^{\infty}_{g\,lim}$, is independent of time. Larive's results demonstrated that the strain (ASR swelling) corresponding to the pressure induced by the ASR gel reaches a maximum value after sufficient time. Figure 13 illustrates a schematic form obtained from Larive's results on ASR swelling with a maximum strain value, ε^{∞}.

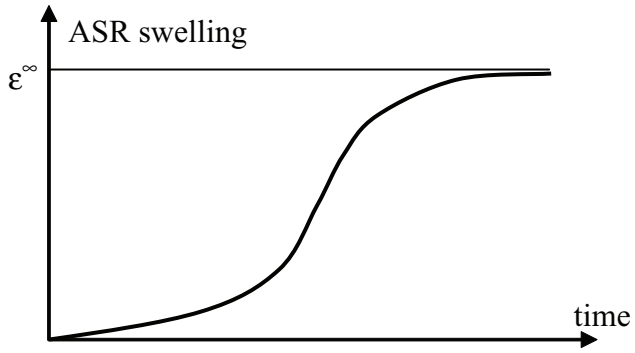

Figure 13. ASR Swelling Evolution as A Function of Time

8.0 FREEZING AND THAWING

Concrete structures that are exposed to harsh winter conditions can undergo several types of degradation such as micro-cracking and structural cracking (Leger et al. 1995). Micro-cracking can result from water movement within the material during the freezing process and structural cracking can result from temperature gradients throughout the structure.

Micro-cracking induced by the freeze/thaw (F/T) cycling can have a detrimental effect on the service behavior of concrete structures. It affects the physical, chemical, and mechanical properties of the concrete and often causes surface spalling.

The frost resistance of cement pastes was the topic of many model developments dedicated to the prediction of damage to concrete structures exposed to freezing/thawing cycles. The mechanisms by which freeze/thaw cycling affects the concrete durability are complex and modeling must take into account a wide range of more or less coupled multi-scale phenomena (Scherer 1993 and Marchand et al. 1995). Several models have been proposed to predict the behavior of cementitious materials exposed to freezing conditions (Scherer 1999, Setzer 2000 and Setzer 2001). A numerical model was also developed by Zuber (Zuber and Marchand 2000 and Zuber 2002) to predict the quantity of ice formed in a saturated material as well as the expansion caused by the ice formation.

Moreover, many experiments have also been developed to evaluate the durability of concrete subject to freezing (Pigeon and Pleau 1995). Although some of these tests provide data on the behavior of cementitious materials under freezing conditions, they cannot be used to predict the service life for structures since laboratory conditions do not accurately replicate real conditions (Litvan 1978). During these tests, the concrete samples are usually saturated and exposed to freezing conditions to accelerate degradation. In practice, however, most structures are exposed to drying and wetting cycles that maintain materials in a partially saturated state.

It is well-known that the frost resistance of concrete can be improved by adding air entraining agents in the mixture. Air bubbles inside of concrete act to absorb the pressure induced by ice formation. Many studies were carried out in recent years to describe the effect of air entrainment on the F/T resistance of concrete (Powers 1949 and Pigeon et al. 1996). The Powers' model of the critical spacing factor of air voids has been widely used to quantify the F/T resistance of concrete.

8.1 Ice Formation Mechanism

As temperature inside concrete decreases below the freezing point, the pore solution freezes gradually. The ice formation process is accompanied by heat release that can be detected at low temperatures by calorimetry (Zuber 2002).

Figure 14 shows typical results from calorimetric testing. The testing temperatures vary over a sufficient range to ensure that heat release, throughout the testing, was not due to inherent kinetic problems. Therefore, the heat release recorded by the calorimeter was related to the progressive formation of ice in the porous material (Bager 1986a, Zuber 2002 and Kaufman 2004).

Various stages can be distinguished during a calorimetric test from the location of the main heat release. The ice formation process depends on the pore size distribution (Brun 1977, Matala 1995, Zuber 2002). The first heat peak, appearing between 0°C and -15°C, corresponds to the formation of ice within the largest capillary pores. The heat release observed in the -15°C to -35°C range corresponds to the formation of ice in the nanometer-sized hydrate pores. The last heat peak is related to the freezing of the liquid phase present in the C-S-H interlayer space.

During the ice formation process, water expands by approximately 9% of its volume (Kaufman 2004). This phenomenon has a direct consequence on the material's behavior since the expansion generates internal pressures. Through expansion testing, the evolution of macroscopic deformation caused by F/T cycling can be monitored. In general, a material expands when heated up and contracts when cooled down. When a saturated porous material is cooled down, contraction is observed. However, when ice is formed within the material, expansion takes place. Obviously, this type of volumetric instability cannot be connected solely to deformations of a purely thermal nature. Moreover, the expansion can induce deterioration in the material due to unrecoverable deformations.

From Figure 15, it can be seen that the expansion is greater in pastes with higher w/c ratios. The main reason is that these materials have normally a higher porosity and contain a larger volume of freezing water (see Figure 14).

8.2 F/T Cycle Damage and Saturation

When porous materials are unsaturated, ice formation is decreased: the material properties are less effected and the related expansion is significantly reduced (Litvan 1978). Moreover, the unsaturated pores can potentially act like air-entrained bubbles and decrease the pressure induced by ice formation. Through calorimetric measurements, Bager (1986b and 1987) also concluded that water content contributes to ice formation in porous materials.

Repeated freezing/thawing cycles damage the material, which contributes to pore volume expansion and reduces the mechanical resistance. Fagerlund (2004) quantified the effect of saturation on the damage sustained by cementitious materials exposed to frost action. He determined that there is a critical saturation level where no damage is observed. Above this threshold, damage can be observed. The extent of damage depends on the saturation level and the number of cycles:

$$\delta = \begin{cases} 0 & \text{if} \quad S_r \le S_{cr} \\ K_N \, (S_r - S_{cr}) & \text{if} \quad S_r > S_{cr} \end{cases} \qquad (102)$$

where: δ is the damage parameter due to F/T cycles, S_r is the degree of saturation, S_{cr} is the critical degree of saturation and K_N is the coefficient of fatigue:

$$K_N = \frac{A_c \cdot N_c}{B_c + N_c} \qquad (103)$$

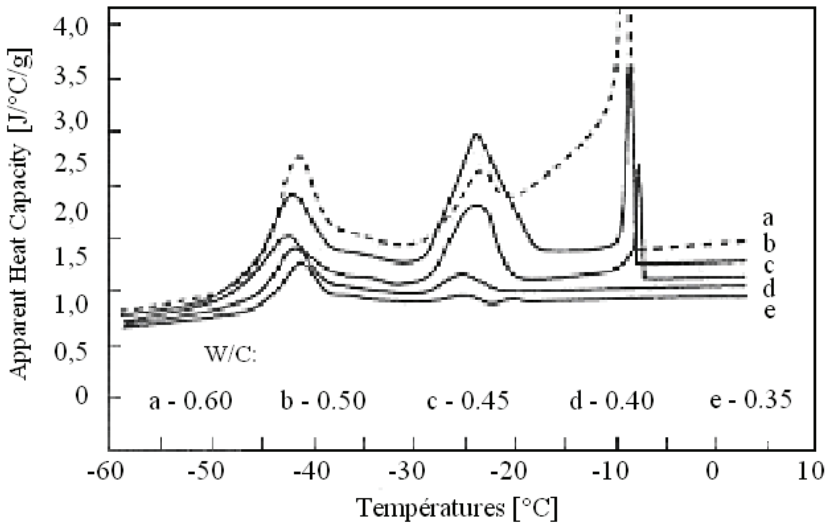

Figure 14. Heat Released from Ice Formation Experiments on Saturated Cement Pastes at Various Water/Cement Ratios (Bager 1986a)

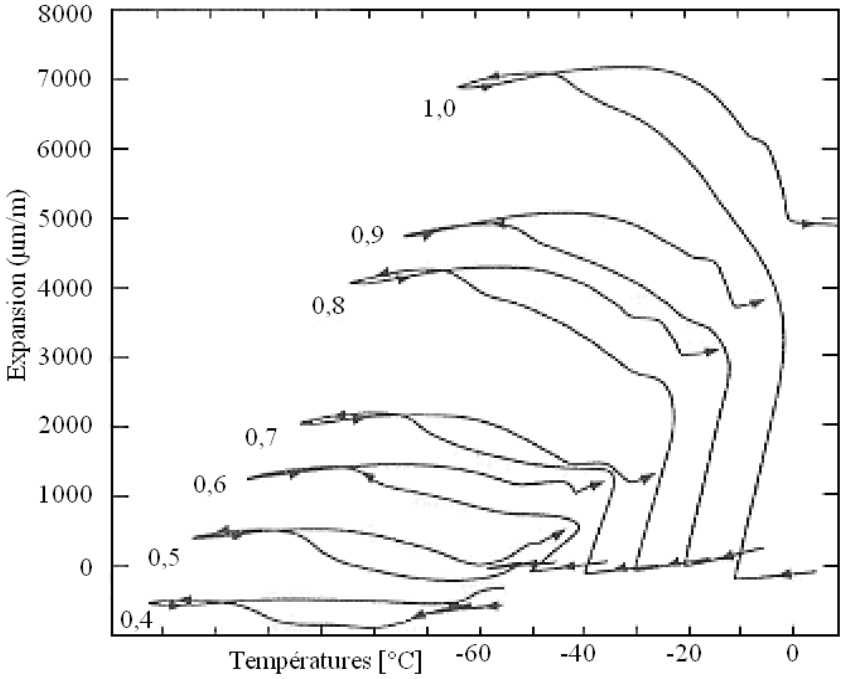

Figure 15. Expansion of Saturated Cement Pastes with Various w/c Ratios (Litvan 1978)
(The start point of all curves is 0°C but they are moved just for comparison.)

N_c is the number of cycles for $S_r > S_{cr}$, and A_c and B_c are two material parameters depending on concrete type. A_c and B_c can be obtained by the fitting curve of K_N versus several N (see Figure 16). This equation is calibrated for a closed system and is valid for a small N_c. For large values of N_c, B_c does not have any influence on K_N and the limit of K_N approaches A_c. In this case, Fagerlund replaced K_N by:

$$K_N = \gamma_c \cdot N_c \tag{104}$$

where: γ_c is the rate of saturation increase, which is different in an open or closed system.

Based on Rombén's experimental results (Fagerlund 2004), the critical degree of saturation was estimated to be between 0.75 and 0.8. As shown in Figure 16, the ratio of the damaged dynamic Young's modulus (E_n) for N cycles of freezing and thawing to the initial undamaged dynamic Young's modulus (E_0) starts to decrease after critical saturation. Moreover, the slope of the curve after critical saturation depends on the number of F/T cycles. For a structure without any existing or historic results that can show the amount of F/T cycles the structure has undergone, N could perhaps be estimated by relating to some experimental relationship. For example, Houvinen (1993) devised an empirical equation that is based on the change of concrete tensile strength:

$$Log\ N = 13.92 - 14.42\ \frac{f_t}{f_t^{\ max}} \tag{105}$$

where: f_t is the tensile strength between cement and aggregates subject to repeated loading, and f_t^{max} is the tensile strength between cement and aggregates subject to static loading.

8.3 Effect of W/C on F/T Damage

The method described in the last section is sufficient for determining the relation between freezing/thawing cycles and damage parameters. According to Fagerlund's approach, the F/T damage is only a function of the number of cycles. But the characteristics of concrete were not considered in the relationship. One of the most important parameters that can affect the damage is the w/c ratio. Many experimental results showed the relation between w/c ratio and F/T damage produced in materials. Figures 17(b) and (c) show the evolution of the dynamic Young's modulus with F/T cycles obtained by Setzer (2001) and Pinto and Hover (cited in Kosmatka

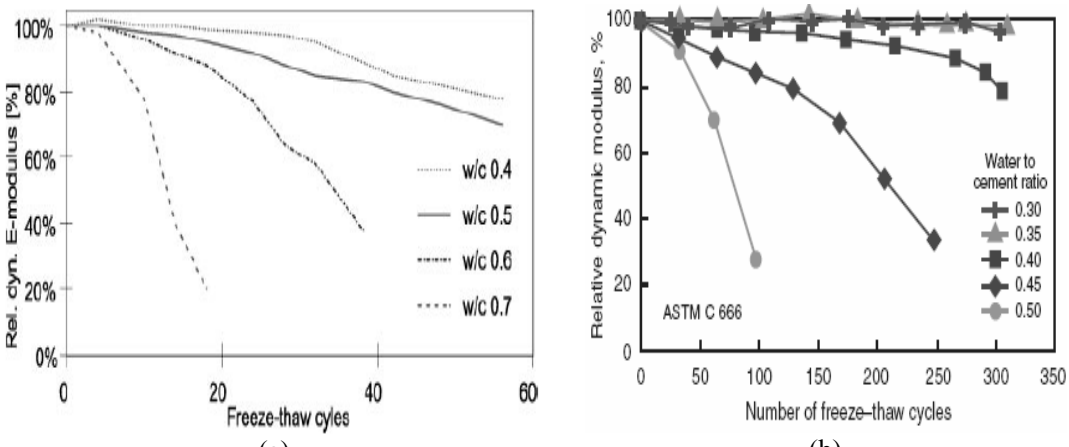

Figure 16. Relative Dynamic Young's Modulus Evolution vs. Freezing/Thawing Cycles According to Rombèn's Results (Fagerlund 2004)

2002), respectively. Sun et al. (1999) also studied the F/T damage under mechanical loading in different concrete types. Figure 17(c) shows their results for F/T damage on four different concrete types, PC40, PC50, PC60, and PC80 corresponding to w/c ratios of 0.45, 0.38, 0.32, and 0.26, respectively.

8.4 Cooling Rate

Freeze/thaw cycle characteristics such as the rate of cooling also influence the damage induced by ice formation. A rapid cooling rate will likely cause more damage to the material (Jacobsen et al.1997). During freezing, the pore solution can be readily transformed into ice and create strain in the material. Greater expansion occurs for faster cooling rates when the material is saturated and also when spacing factors and porosities are higher. These deformations affect the porous network at different scales. The porous network can therefore be changed during one F/T cycle and have different properties for subsequent cycles.

8.5 Pore Pressure Evolution as A Function of Ice Formation

The study of the evolution of pore pressure with freezing is necessary in order to establish a coupled thermo-hydro mechanical model. The continuum

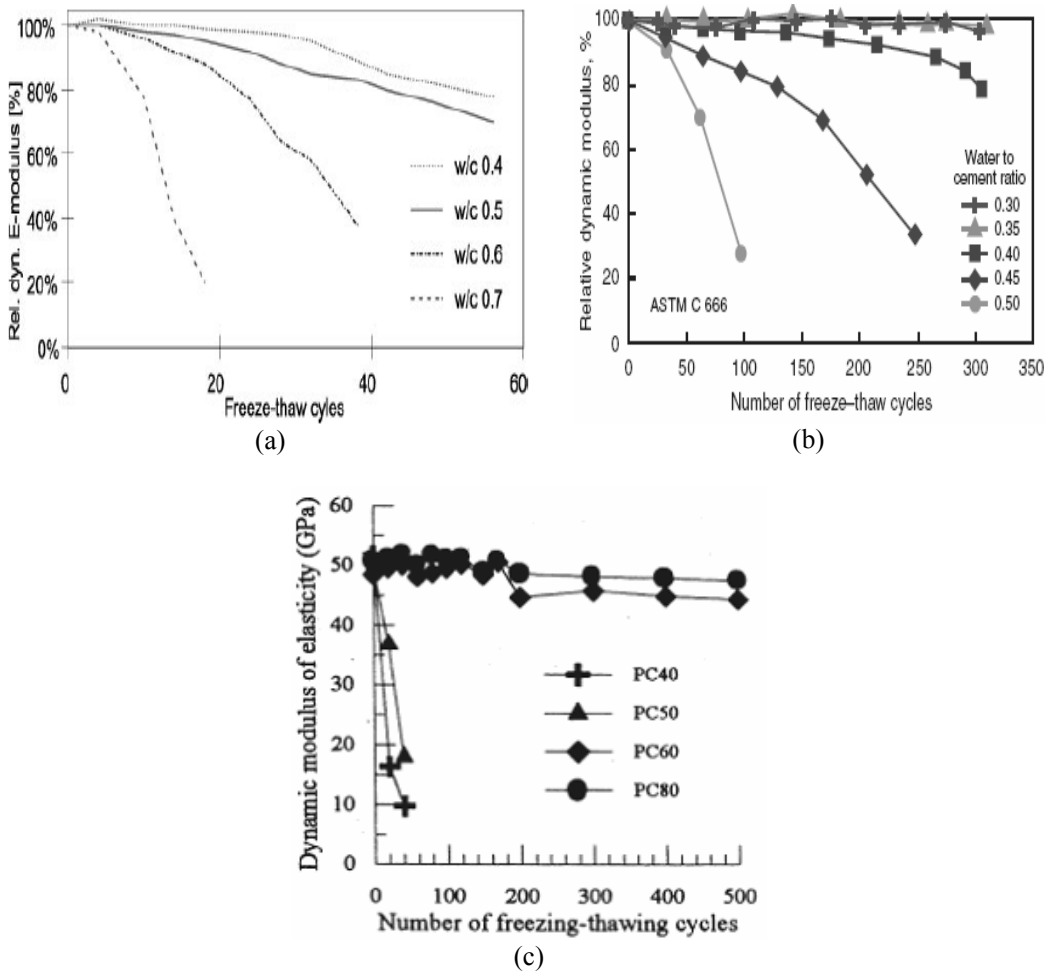

Figure 17. Evolution of Damage as A Function of the F/T Cycles

mechanics of porous media can be used as a theoretical basis for the internal stress calculations. According to Coussy (1995), the effective stress inside thematerial can be written as:

$$\sigma = \sigma' - b\, p\, I \tag{106}$$

In this equation, σ and σ' are total and effective stress, respectively, p is the internal homogenized pore pressure, b is the Biot coefficient, and I is the unit matrix.

Pressure evolution p can be determined from micro-scale studies and extended to the macro-scale by a homogenization on an equivalent representative volume. This pressure is the sum of liquid pressure p_l and the pressure induced by ice formation p_{ice} and is applied as the total pore pressure in the hydrous analysis of porous media:

$$p = p_l + p_{ice} \tag{107}$$

Expressions for the pressure contribution p_{ice} is given for saturated and unsaturated porous materials below.

8.5.1 Saturated Porous Media

Zuber (2002) proposed an expression for the pressure generated by ice formation for cylindrical shaped pores. According to this approach, there exists an equilibrium pore radius Req at a given freezing temperature and pore solution concentration, for which larger pores are frozen and smaller ones are not. For this equilibrium radius, the contribution of ice on the total pressure exerted on the pore walls is given by:

$$p_{ice} = \frac{1}{\phi}\int_{\infty}^{R_{eq}} \gamma_{ls}\left(\frac{2}{R_{eq}} - \frac{1}{r - l_r}\right)\frac{\mathrm{d}\varphi(r)}{\mathrm{d}r}\,\mathrm{d}r \tag{108}$$

where: γ_{ls} is the surface tension between liquid and solid phases, l_r is the thickness of the adsorbed layer in the porous system, ϕ is the porosity, and $\varphi\,(r)$ is the pore size distribution.

This approach has the advantage that it considers the effects of surface tension between solid and liquid phases. However, it relies on a physically unrealistic uniform cylindrical pore shape geometry.

Penttala (2002) established an expression in which the total liquid phase pressure can be calculated in a frozen porous media. The geometry of the pores was not considered in this approach, which provides a homogenized pressure:

$$p = \frac{\Delta h_0^{ls}}{\left(v_s - v_l\right)T}\Delta T + \frac{1}{\left(v_s - v_l\right)}\int_{T_0}^{T}\int_{T_0}^{T}\frac{c_p^s - c_p^l}{T}dTdT \tag{109}$$

where: c_p^s and c_p^l are the heat capacity for ice and water, respectively; v_s and v_l are the specific volume of ice formation and water, respectively, Δh_0^{ls} is the enthalpy of ice formation, and T_0 and T are the initial and the current temperatures.

8.5.2 Unsaturated Porous Media

The water content can play an important part in the quantity of ice formed (Bager and Sellevold 1986b and 1987) and, consequently, in the service life of concrete (Fagerlund 2000). This factor must be accounted for the F/T models. In addition, the beneficial aspect of air bubbles should also be taken into account because these beneficial effects dissipate the pressures generated in porosity. However, few studies that have been conducted on pore pressure expressions during freezing of unsaturated materials.

Penttala (1998 and 2002) proposed an expression for pore pressure that also depends on the ionic species characterized by the molar fraction x_{unf} and the activity of the liquid phase a_l.

$$p = \frac{RT}{v_s} ln\left(\frac{RH}{a_l x_{unf}}\right) + \frac{\Delta h_0^{ls}}{v_s T_0}\Delta T + \frac{1}{v_s}\int_{T_0}^{T}\int_{T_0}^{T}\frac{c_p^s - c_p^l}{T} dT dT \quad (110)$$

where RH is the relative humidity, depending on the vapor and the saturated vapor pressures p_v and p_{vs}, R is the gas constant and $RH = \frac{p_v}{p_{vs}(T)}$. For an ideal solution, the molar fraction x_{unf} and the chemical activity a_l are both equal to 1. Adsorption/desorption isotherm tests can be used to determine the water content from relative humidity evolution (Xi et al. 1994).

9.0 CONCLUSIONS

This review of approaches to modeling mechanical damage in cementitious materials emphasized a clear preference toward damage mechanics, where the degradation is quantified using a damage tensor that affects the mechanical properties such as Young's modulus. No models based on fracture mechanics used in the context of concrete durability were reviewed for this report.

The review showed that it is possible to couple damage mechanics models to ionic transport equations in order to get a global durability that would be well suited for the purposes of the Cementitious Barrier Partnership project. In all cases, the mechanical and mass exchange portions of the models are solved separately, with the output of one module being used to calculate or update inputs in another. Although the papers reviewed in this report were mostly based on simplified transport equations, the splitting between transport and mechanics makes it possible to envision more complex transport models linked to damage-based modules.

10.0 REFERENCES

ACI Concrete Repair Manual. 2007, 'Causes, Evaluation, and Repair of Cracks in Concrete Structures', ACI 224.1R-07.

ACI Concrete Repair Manual. 2007, 'Nondestructive Test Methods for Evaluation of Concrete in Structures', ACI 228.2R-98.

ACI Manual of Concrete Practice 2008, 'Finite element analysis of fracture in concrete structures', ACI 446.3R-97.

ACI Manual of Concrete Practice 2008, 'Prediction of creep, shrinkage, and temperature effects in concrete structures', ACI 209R-92.

ACI Manual of Concrete Practice 2008, 'Report on factors affecting shrinkage and creep of hardened concrete', ACI 209.1R-05.

ACI Manual of Concrete Practice 2008, 'Control of cracking in concrete structures', ACI ACI 224R-01.

Achintya, M & Prasad, MM 2003, 'Behavior of Concrete in Freeze-thaw Environment of Sea Water', Technical Journals of the Institution of Engineering (India), vol. 84.

Ahmad, S 2003, 'Reinforcement corrosion in concrete structures, its monitoring and service life prediction', Cement & Concrete Composites, vol. 25, pp. 459-471.

ASTM 2008, 'Concrete and aggregates', Annual book, vol. 04.02.

Atkinson, A & Hearne, J A 1989, 'Mechanistic model for the durability of concrete barriers exposed to sulfate bearing ground water', Scientific Basis for Nuclear Waste Management, vol. 13, pp. 149-156.

Bager, DH & Sellevold, E 1986a, 'Ice formation in hardened cement paste, part I: room temperature cured pastes with variable moisture contents', Cem. & Conc. Res., vol. 16, pp. 709-720.

Bager, DH & Sellevold, E 1986b, 'Ice formation in hardened cement paste, part II: drying and resaturation on room temperature cured pastes', Cem. & Conc. Res., vol. 16, pp. 835-844.

Bager, DH & Sellevold, E 1987, 'Ice formation in hardened cement paste, part III: slow resaturation of room temperature cured paste', Cem. and Conc. Research, vol. 17, pp. 1-11.

Basista, M 2001, 'Micromechanical and lattice modeling of brittle damage', Institute of Fundamental Technological Research, Warsaw, Poland.

Basista, M & Weglewski, W 2008, 'Chemically-assisted damage of concrete: a model of expansion under external sulfate attack', J. of Theor. and App. Mechanics, vol. 35, pp. 29-52.

Bazant, ZP 2001, 'Prediction of concrete creep and shrinkage: past, present and future', Nuclear Engineering and Design, vol. 203, pp. 27–38.

Bazant, ZP Xian, Y & Prat, PC 1996, 'Microplane model for concrete. Part I and II', J. of Eng. Mechanics - ASCE, pp. 245-262.

Benboudjema, F Meftah, F & Torrenti, JM 2005, 'Interaction between drying, shrinkage, creep and cracking phenomena in concrete', Eng. Structures, vol. 27, pp. 239–250.

Benboudjema, F & Torrenti, JM 2008, 'Early-age behaviour of concrete nuclear containments', Nuclear Engineering and Design, vol. 238, pp. 2495–2506.

Bentz, D P Coveney, P V & Garboczi, E J 1994, 'Cellular automaton simulations of cement hydration and microstructure development', Modelling and Simulation in Materials Science and Engineering, vol. 2, pp. 783-808.

Bérubé, MA Chouinard, D Pigeon, M Frenette, J Rivest, M & Vézina, D 2002a, 'Effectiveness of Sealers in Counteracting Alkali-Silica Reaction in Highway Median Barriers Exposed to Wetting and Drying, Freezing and Thawing, and Deicing Salts', Canadian Journal of Civil Engineering, vol. 29, pp. 329-337.

Bhargava, K Ghoshb, AK Moric, Y & Ramanujama, S 2006, 'Model for cover cracking due to rebar corrosion in RC structures', Engineering Structures, vol. 28, pp. 1093-1109.

Bouchard, PO Bay, F & Chastel, Y 2003, 'Numerical modelling of crack propagation: automatic remeshing and comparison of different criteria', Comput. Methods Appl. Mech. Eng., vol. 192, pp. 3887–3908.

Brun, M Lallemand, A Quinson, JF & Eyraud, C 1977, 'A new method for the simultaneous determination of the size and the shape of pores: The thermoporometry', Thermochimica Acta, vol. 21, pp. 59-88,

Budiansky, B & O'Connell, R J 1976, 'Elastic moduli of a cracked solid', International Journal of Solids and Structures, vol. 12, pp. 81-97.

Buyukozturk, O & Hearing, B 1998, 'Crack propagation in concrete composites influenced by interface fracture parameters', Int. J Solids Struc., vol. 35, pp. 4055-4066.

Capra, B & Sellier, A 2003, 'Orthotropic modelling of alkali-aggregate reaction in concrete structures: numerical simulations', Mechanics of Materials, vol. 35, pp. 817–830.

Carol, I & Bazant, ZP 1991, 'Geometric damage tensor based on microplane model', Journal of Engineering Mechanics, vol. 117, pp. 2429-2448.

Cervera, M Olivier, J & Prato, T 1999, 'Thermo-chemo-mechanical model for concrete. I: Hydration and aging', Journal of Engineering Mechanics, vol. 125, pp. 1018-1027.

Cervera, M Olivier, J & Prato, T 1999b, 'Thermo-chemo-mechanical model for concrete. II: Damage and creep', Journal of Engineering Mechanics, vol. 125, pp. 1018-1027.

Chatterji, S 1999, 'Aspects of the freezing process in a porous material - part 1: Freezing and the properties of water and ice', J. of Cem. and Conc. Res., vol. 29, pp 627–630.

Chatterji, S 2005, 'Chemistry of alkali–silica reaction and testing of aggregates', Cement & Concrete Composites, vol. 27, pp. 788-795.

Chen, D & Mahadevan, S 2008, 'Chloride-induced reinforcement corrosion and concrete cracking simulation', Cement and Concrete composites, vol. 30, pp. 227-238.

Chiarelli, AS Shao, JF & Hoteit, N 2003, 'Modeling of elastoplastic damage behavior of claystone', International Journal of Plasticity, vol. 19, pp. 23-45.

Clifton, JR & Pommersheim, JM 1994, 'Sulfate attack of cementitious materials: Volumetric relations and expansions Technical report, Building and Fire Research Laboratory', National Institute of Standards and Technology, Gatheirsburg, MD.

Contecvet manual 2001, 'A validated Users Manual for assessing the residual service life of concrete structures', Lund University - Division of Building Materials.

Collepardi, M 2003, 'A state-of-the-art review on delayed ettringite attack on concrete', Cement and Concrete Composites, vol. 25, pp. 401-407.

Coussy, O 1995, 'Mechanics of porous continua', John Wiley & Sons.

Dekoster, M Buyle-Bodin, F Maurel, O & Delmas, Y 2003 'Modelling of the flexural behaviour of RC beams subjected to localised and uniform corrosion', Engineering Structures, vol. 25, pp. 1333-1341.

Dent Glasser, LS & Kataoka, N 1981, 'The chemistry of alkali-aggregate reaction', Cement and Concrete Researchm, vol. 11, pp. 1-9.

Diamond, S Barneyback, RS & Struble, LJ 1981, 'On the physics and chemistry of alkali-silica reactions', Proceedings of the 5th Int. Conf. on Alkali-Aggregate Reaction in Concrete - Cape Town (South Africa), pp. 252.

Diamond, S 2000, 'Chemistry and other characteristics of ASR gels', Proceedings of the 11th Int. Conf. on Alkali-Aggregate Reaction in Concrete, edited by Bérubé et al., Québec (CANADA), pp. 31-40.

Dragon, A Halm, D & Desoyer, Th 2000, 'Anisotropic damage in quasi-brittle solids: modeling, computational issues and applications', Comput. Meth. Appl. Mech. Eng., vol. 183, pp. 331-352.

Du, YG Chan, AHC & Clark, LA 2006, 'Finite element analysis of the effects of radial expansion of corroded reinforcement', Computers and Structures, vol. 84, pp. 917-929.

Duchesne, J & Bérubé, MA 2000, 'Long-term effectiveness of supplementary cementing materials against ASR', Proceedings of the 11th Int. Conf. on Alkali-Aggregate Reaction in Concrete, edited by Bérubé et al., Québec (CANADA), pp. 613-622.

Espenson, JH 1981, 'Chemical kinetics and reaction mechanisms', McGraw-Hill.

Fagerlund, G 2000, 'Mechanical damage and fatigue effects associated with freeze-thaw of materials', RILEM PRO 24, Frost Resistance of Concrete, pp. 117-132.

Fagerlund, G 2004, 'A service life model for internal frost damage in concrete', Lund University publishing, Sweden.

Folliard, KJ Thomas, MDA & Kurtis, K 2003, 'Guidelines for the use of lithium to mitigate or prevent ASR', FHWA-RD-03-047, Federal Highway Administration, National Research Council, Washington D.C.

Fournier, B & Bérubé, MA 2000, 'Alkali-aggregate reaction in concrete: a review of basic concepts and engineering applications', Canad. J. of Civ. Eng., vol. 27, pp. 167-191.

Fu, Y Xie, P & Beaudoin, JJ 1994, 'Significance of pre-existing cracks on nucleation of secondary ettringite in steam cured cement paste', Cem.& Conc. Res., vol. 24, pp. 1015-1024.

Garboczi, E J & Bentz, DP 1992, 'Computer simulation of the diffusivity of cement-based materials', Journal of Material Sciences, vol. 27, pp. 2083-2092.

Garboczi, EJ & Bentz, DP 2001, 'The effect of statistical fluctuation, finite size error, and digital resolution on the phase percolation and transport aspects of the NIST cement hydration model', Cem. Conc. Res. ,vol 31, pp. 1501-1514.

Gawin, D Pesavento, F & Schrefler, BA 2006, 'Hygro-chemo-mechanical modeling of concrete at early ages and beyond. Part I: Hydration and hygro-thermal phenomena', Int. J. Num. Meth. Eng., vol. 67, pp.299-331.

Gerard, B 1996, 'Contribution des couplages mécaniques-Chimie-Transfert dans la tenue à long term des ouvrages de stockage de déchets radioactifs', Ph.D. thesis of ENS Cachan – France and Laval University of Québec – Canada.

Gerard, B Pijaudier-Cabot, G & Laborderie, C 1998, 'Coupled Diffusion – Damage modeling and the implications on failure due to strain localization', International Journal Solids Structures, vol. 35, pp. 4107-4120.

Gerard, B & Marchad, J 2000, 'Influence of cracking on the diffusion properties of cement-based materials Part I: Influence of continuous cracks on the steady-state regime', Cement and Concrete Research, vol. 30, pp. 37-43.

Glasser, FP 1992, 'Chemistry of the alkali-aggregate reaction, in Concrete', R.N. Swamy ed., Blackie (Glasgow, UK), pp. 30-53.

Gospodinov, P Kazandjiev, R & Mironova, M 1996, 'The effect of sulfate ion diffusion on the structure of cement stone', Cement and Concrete Composites, vol. 18, pp. 401-407.

Halm, D & Dragon, A 1998, 'An anisotropic model of damage and frictional sliding for brittle materials', European Journal of Mechanics and Solids, vol. 17, pp. 439-460.

Helmuth, RA & Stark, D 1992, 'Alkali silica reactivity mechanisms', Materials Science of Concrete, J.P. Skalny ed., American Ceramic Society, Westerville (OH), pp. 131-208.

Hou, X Struble, LJ & Kirkpatrick, RJ 2004, 'Formation of ASR gel and the roles of C-S-H and portlandite', Cement Concrete Res., vol. 34, pp. 1683-1696.

Houvinen, S 1993, 'Abrasion of concrete by ice', Journal of Cement and Concrete Research, vol. 23, pp. 68-82.

Hua, C Acker, P & Ehrlacher A 1995, 'Analyses and models of the autogenous shrinkage of hardening cement paste', Cement and Concrete Research, vol. 25, pp. 1457-1468.

IUPAC 1997, 'Compendium of Chemical Terminology', 2nd Edition, Editors: McNaught and Wilkinson.

Jacobsen, S Saether, D & Sellevod, E 1997, 'Frost testing of high strength concrete: frost/salt scaling at different cooling rates', Materials and structures, vol. 30, pp. 33-42.

Jun, W Xianghao, W & Xialong, Z 2003, 'A model for concrete durability degradation in freezing-thawing cycles', Acta Mechanica Solida Sinica, vol. 16, no. 4, pp353-358.

Kachanov, M 1993 'Elastic solid with many cracks and related problems', Advances in Applied Mechanics, vol. 30, pp. 259-445

Kalousek, G 1944, 'Studies of portions of the quaternary system soda-lime-silica-water at 25°C', Journal of Research of the National Bureau of Standards, vol.32, pp. 285-302.

Karihaloo, B L 1995, 'Fracture mechanics and structural concrete', Longman Scientific and Technical, Harlow, Essex, England.

Kaufman, J 2004, 'Experimental identification of ice formation in small concrete pores', Cement and Concrete Research, vol. 34, pp. 1421-1427.

Kim, HS & Cho, SH 2004, 'Shrinkage stress analysis of concrete slabs with shrinkage strips in a multistory building', Computers and Structures, vol. 82, pp. 1143–1152.

Korhonen, C 2002, 'Effect of High Doses of Chemical Admixtures on the Freeze–Thaw Durability of Portland Cement Concrete', US Army Corps of Engineers.

Kirkpatrick, RJ Kalinichev, AG Hou, X & Struble, L 2005, 'Experimental and molecular dynamics modeling studies of interlayer swelling: water incorporation in kanemite and ASR gel', Materials and Structures, vol. 38, pp. 449-458.

Knudsen, T & Thaulow, N 1975, 'Quantitative microanalysis of alkali-silica gel in concrete', Cement and Concrete Research, vol. 5, pp. 443-454.

Kosmatka, S Kerkhof, B & Panarese, W 2002, 'Design and Control of Concrete Mixtures', Portland Cement Ass., Skokie, Illinois, Item Code: EB001, 14th Edition.

Krajcinovic, D Basista, M Mallik, K & Sumarac, D 1992, 'Chemo-micromechanics of brittle solids', Journal of Mechanics and Physics of Solids, vol. 40, pp. 965-990.

Kurtis, KE Monteiro, PJM Brown, JT & Meyer-Ilse, W 2004, 'Mechanisms of concrete damage caused by sulfate attack examined through transmission x-ray microscopy', Adv. Light Source Compendium of User Abstracts (https://www.als.lbl.gov/als/compendium)

Léger, P Côté, M & Tinawi, R 1995, 'Thermal protection of concrete dams subjected to freeze-thaw cycles', Canadian Journal of Civil Engineering, vol. 22, pp. 588-602.

Lemaitre, J Demorat, R & Sauzay, M 2000, 'Anisotropic damage law of evolution', Eur. J. Mech., vol. 19, pp. 187-208.

Lemaitre, J & Chaboche, JL 1985, 'Mécanique des matériaux solides', Dunod Editions.

Li, K Ulm, FJ Coussy, O Larive, C & Fan, L 2000, 'Chemoplastic modeling of alkali-silica reaction in concrete', Proceedings of the 11th Int. Conf. on Alkali-Aggregate Reaction in Concrete, edited by Bérubé et al., Québec (CANADA), pp. 989-998.

Li, K & Coussy, O 2002, 'Concrete ASR degradation: from material modeling to structure assessment', Concrete Science and Engineering, vol. 4, pp. 35-46.

Litvan, GG 1978, 'Adsorption systems at temperatures below the freezing point of the adsorptive', Advances in Colloid and Interface Science, vol. 9, pp. 253-302.

Liu, Y & Weyers, R 1998, 'Modeling the time-to-corrosion cracking in chloride contaminated reinforced concrete structures', ACI material journal of Nov-Dec.

Marchand, J 2001, 'Modeling the behavior of unsaturated cement systems exposed to aggressive chemical environments', Materials and Structures, vol. 34, pp. 195-200.

Marchand, J Pleau, R & Gagné, R 1995, 'Deterioration of concrete due to freezing and thawing', Materials Science of Concrete, pp. 283-354.

Marchand, J Samson, E Maltais, Y & Beaudoin, JJ 2002, 'Theoretical analysis of the effect of weak sodium sulfate solutions on the durability of concrete', Cement and Concrete Research, vol. 24, pp. 317-329.

Martin-Pérez, B 1999, 'Service life modeling of R.C. highway structures exposed to chlorides', Ph.D. Thesis at University of Toronto.

Matala, S 1995, 'Effects of carbonation on the pore structure of granulated blast furnace slag concrete', PhD thesis of University of Technology, Faculty of Civ. Eng., Espoo, Finland.

Mazars, J & Pijaudier-Cabot, G 1989, 'Continuum damage theory – application to concrete', Journal of Engineering Mechanics, vol. 115, no 2, pp. 345-362.

Mazars, J & Pijaudier-Cabot, G 1996, 'Frome damage to fracture mechanics and conversely: a combined approach', Int. J. Solids Struct., vol. 33, no. 20-22, pp. 3327-3342.

Mehta, PK 1983, 'Mechanism of sulfate attack on portland cement concrete - another look', Cement and Concrete Research, vol. 13, pp. 401-406.

Meschke, G & Grasberger, S 2003, 'Numerical modeling of coupled hygromechanical degradation of cementitious materials', J. of Eng. Mechanics, pp. 383-392.

Millard, MJ & Kurtis, KE 2008, 'Effects of lithium nitrate admixture on early age cement hydration', Cement and Concrete Research, vol. 38, pp. 500-510.

Mindess, S, Young, J F & Darwin, D 2002, 'Concrete', Prentice Hall, 2nd edition.

Multon, S & Toutlemonde, F 2006, 'Effect of applied stresses on alkali-silica reaction-induced expansions', Cement and Concrete Research, vol. 36, pp. 912-920.

Multon, S Cyr, M Sellier, A Leklou, N & Petit, L 2008, 'Coupled effects of aggregate size and alkali content on ASR expansion', Cem. and Conc. Res., vol. 38, pp. 350-359.

Mura, T 1987, 'Micromechanics of defects in solids', Martinus Nijhoff Publications, The Hague, Netherlands.

Penttala, V 1998, 'Freezing-Induced Strains and Pressures in Wet Porous Materials and Especially in Concrete Mortars', Advanced Cement Based Materials, vol. 7, pp. 8-19.

Penttala, V 2002, 'From freezing and thawing pore water pressures to concrete stresses', RILEM PRO 24, Frost Resistance of Concrete, pp. 147-160.

Picandet, V Khelidj, A & Bastian, G 2001, 'Effect of axial compressive damage on gas permeability of ordinary and high-performance concrete', Cement and Concrete Research, vol. 31, pp. 1525-1532.

Pigeon, M & Pleau, R 1995, 'Durability of Concrete in Cold Climates', Modern Concrete Technology series Published by Taylor and Francis, vol. 4.

Pigeon, M Marchand, J & Pleau, R 1996, 'Frost resistant concrete', Construction and Building Materials, vol. 10, pp. 339-348.

Ping, X & Beaudoin, JJ 1992, 'Mechanism of sulfate expansion I. thermodynamic principle of crystallization pressure', Cement and Concrete Res., vol. 22, pp. 631-640.

Powers, T 1949, 'The air requirement of frost-resistant concrete', Highway Research Board, vol. 29, pp. 184-211.

Powers, TC & Steinour, HH 1955, 'An interpretation of some published researches on alkaliaggregate reaction 2 – An hypothesis concerning safe and unsafe reactions with reactive silica in concrete', Journal of ACI Proceedings, vol. 51, pp. 785-811.

Prezzi, M Monteiro, PJM & Sposito, G 1997, 'The alkali-silica reaction – Part 1. Use of the double-layer theory to explain the behaviour of reaction-product gels', ACI Materials J., vol. 94, pp. 10-17.

Prezzi, M Monteiro, PJM & Sposito, G 1998, 'The alkali-silica reaction – Part 2. the effect of chemical admixtures', ACI Materials J., vol. 95, pp. 3-10.

Rahman, MK Baluch, MH & Al-Gadhib, AH 2000, 'Simulation of shrinkage distress and creep relief in concrete repair', Composites - Part B: Engineering, vol. 31, pp. 541-553.

Rongbing, B Jian, S 2005, 'Synthesis and evaluation of shrinkage-reducing admixture for cementitious materials', Cement and Concrete Research, vol. 35, pp. 445– 448.

Rostasy, FS & Weidemann, G 1980, 'Stress-Strain-Behaviour of concrete at extremely low temperature', Journal of cement and concrete research, vol. 10, pp. 565-572.

Saetta, A Scotta, R & Vitaliani, R 1998, 'Mechanical behavior of concrete under physical-chemical attacks', Journal of Engineering Mechanics, vol. 1240, pp. 1100-1109.

Salganik, RL 1973, 'Mechanics of bodies with many cracks', Mechanics of Solids, vol. 8, pp. 135-143.

Samson, E & Marchand, J 1999, 'Numerical solution of the extended nernst-plack model', Journal of Colloid and Interface Science, vol. 215, pp. 1-8.

Samson, E Lemaire, G Marchand, J & Beaudoin, JJ 1999a, 'Modeling chemical activity effects in strong ionic solutions', Computational Materials Sci., vol. 15, pp. 285-294.

Samson, E Marchand, J & Beaudoin, JJ 1999b, 'Describing ion diffusion mechanisms in cement-based materials using homogenization technique', Cement and Concrete Research, vol. 29, pp. 1341-1345.

Samson, E Marchand, J Robert, JL & Bournazel, JP 1999c, 'Modeling of ion diffusion mechanisms in porous media', Int. J. of Numerical Methods in Eng., vol. 46, pp. 2043-2060.

Samson, E Marchand, J & Snyder, KA 2003, 'Calculation of ionic diffusion coefficients on the basis of migration test results', Materials and Structures, vol. 36, pp. 156-165.

Santhanam, M Cohen, MD & Olek, J 2001, 'Review: sulfate attack research - whither now', Cement and Concrete Research, vol. 31, pp. 845-851.

Scherer, GW 1993, 'Freezing gels', Journal of Non-Crystalline Solids, vol.155, pp. 1-25.

Scherer, GW 1999, 'Crystallization in pores', Cem. and Conc. Res., vol. 29, pp. 1347-1358.

Schmidt-Dohl, S & Rostasy, FS 1999, 'A model for the calculation of combined chemical reactions and transport processes and its application to the corrosion of mineral-building materials part I. simulation model', Cement and Concrete Res., vol. 29, pp. 1039-1045.

Scrivener, KL & Monteiro, PJ 1994, 'The alkali silica reaction in a monolithic opal', Journal of the American Ceramic Society, vol. 77, pp. 2849-2856.

Sellevold, E Jacobsen, S & Bakke, J 1997, 'High-strength concrete without air entrainment: Effect of rapid temperature cycling above and below 0°C', Freeze-thaw durab. of conc. Ed. Marchand J., Pigeon M. and Setzer M., Ste-Foy, Québec, pp. 43-50.

Setzer, M 2000, 'Mechanical Stability Criterion, Triple-Phase Condition, and Pressure Differences of Matter Condensed in a Porous Matrix', Journal of Colloid and Interface Science, vol 235, pp 170-182.

Setzer, M 2001, 'Micro-Ice-Lens Formation in Porous Solid', Journal of Colloid and Interface Science, vol. 243, pp 193–201.

Shao, JF Lu, YF & Lydzba, D 2004, 'Damage modeling of saturated rock in drained and undrained conditions', Journal of Engineering Mechanics ASCE, pp. 733-740.

Shimada, Y Johansen, VC Miller, FM & Mason, TO 2005, 'Chemical path of ettringite formation in heat-cured mortar and its relationship to expansion: A literature review. Technical report', Portland Cement Association, Skokie, IL.

Shazali, MA Baluch, MH & Al-Gadhib, AH 2006, 'Predicting residual strength in unsaturated concrete exposed to sulfate attack', Journal of Materials in Civil Engineering, vol. 180 (3), pp. 343-354.

Snyder, KA 2000, 'Effect of drying shrinkage cracks and flexural cracks on concrete bulk permeability', Nat. Inst. of Stand. And Tech. - May edition.

Stanton, TE 1940, 'Expansion of concrete through reaction between cement and aggregate', Proceedings of the ASCE, vol. 66, pp. 1781-1811.

Stark, J & Bollmann, K 1999, 'Delayed ettringite formation in concrete', Nordic Concrete Research.

Sun, W Zhang, YM Yan, HD & Mu R 1999, 'Damage and damage resistance of high strength concrete under the action of load and freeze-thaw cycles', Journal of Cement and Concrete Research, vol. 29, pp. 1519–1523.

Taylor, HFW Famy, C & Scrivener, KL 2001, 'Review: Delayed ettringite formation', Cement and Concrete Research, vol. 31, pp. 683-693.

Thoft-Christensen, P 2000, 'Stochastic modeling of the crack initiation time for reinforced concrete structures', Structures Congress in Philadelphia-May 8-10, 2000.

Thomas, MDA 1996, 'Review of the effect of fly ash and slag on alkali-aggregate reaction in concrete', Building Research Establishment Report, BR314, Construction Research Communications, Ltd., Watford, U.K.

Thomas, MDA Fournier, B Folliard, K Ideker, J & Shehata, M 2006, 'Test methods for evaluating measures for controlling expansion due to alkali-silica reaction in concrete', Cement and Concrete Research, vol. 36, pp. 1842-1856.

Timoshenko, SP & Goodier, JN 1970, 'Theory of Elasticity', McGraw-Hill, New York.

Tixier, R 2000, 'Microstructural development and sulfate attack modeling in blended cement-based materials', PhD thesis, Arizona State University, Phoenix, Arizona.

Tixier, R & Mobasher, B 2003a, 'Modeling of damage in cement-based materials subjected to external sulfate attack I: Formulation', J. of Materials in Civil Eng., vol. 15, pp. 305-313

Tixier, R & Mobasher, B 2003b, 'Modeling of damage in cement-based materials subjected to external sulfate attack ii.comparison with experiments', Journal of Materials in Civil Engineering, vol. 15, pp 314-322.

Tremblay, C Bérubé, MA Fournier, B Thomas, MDA & Stokes, DB 2004, 'Performance of lithium-based products against ASR: application to Canadian reactive aggregates, reaction mechanisms and testing', Proc. 12th Int. Conf. on Alkali-Aggregate Reaction in Concrete, Beijing (China), pp. 668-677.

Ulm, JF & Coussy, O 1995, 'Modeling of thermochemomechanical couplings of concrete at early ages', Journal of Engineering Mechanics, vol. 121, pp. 785-794.

Ulm, JF & Coussy, O 1995, 'Modeling of thermochemomechanical couplings of concrete at early ages', *Journal of Engineering Mechanics*, vol. 121, pp. 785-794.

Ulm, JF & Coussy, O 1998, 'Couplings in early-age concrete: from material modeling to structural design', *Int. J. Solids and Structures*, vol. 35, pp. 4295-4311.

Ulm, FJ Peterson, M & Lemarchand, E 2002, 'Is ASR expansion caused by chemoporoplastic dilatation?', Concrete Science and Engineering, vol. 4, pp. 47-55.

Wang, X & Liu, X 2006, 'Bond strength modeling for corroded reinforcements', *Construction and Building Materials*, vol. 20, pp. 177-186.

Weglewski, W & Basista, M 2005, 'Damage of concrete in chemically aggressive environment: A micromechanical model', *Technical report, Institute of Fundamental Technological Research, Warlaw, Poland*.

Wieker, W Hubert, C & Ebert, R 1996, 'Contribution to the chemical reaction mechanisms of the alkali aggregate reaction', Proc. Of the 10th Int. Conf. on Alkali-Aggregate Reaction in Concrete, Melbourne, Australia, pp. 919-926.

Xi, Y Bazant, Z & Jennings, HM 1994, 'Moisture Diffusion in Cementitious Materials-Adsorption Isotherms', *Advanced Cement Based Materials*, vol. 1, pp. 248-257.

Yang, Z & Chen, J 2004, 'Fully automatic modelling of cohesive discrete crack propagation in concrete beams using local arc-length methods', *Int. J. of Solids and Structures*, vol. 41, pp. 801-826.

Yuan, SC & Harrison, JP 2006, 'A review of the state of the art in modelling progressive mechanical breakdown and associated fluid flow in intact heterogeneous rocks', *Int. J Rock Mech. & Min. Sci.*, vol. 43, pp. 1001-1022.

Zuber, B 2002, 'Numerical modeling of the mechanisms of frost degradation of hydrated cement systems', *Ph.D. thesis of Laval University–Québec-Canada and ENS Cachan-France.*

Zuber, B & Marchand, J 2000, 'Modeling the deterioration of hydrated cement systems exposed to frost action - Part 1: Description of the mathematical model', *Cement and Concrete Research*, vol. 30, pp. 1929-1941.